Ruby Sharma, Sajal Kumar, and Mingzhou Song

## SUPPLEMENTAL MATERIALS

## Fundamental gene network rewiring at the second order within and across mammalian systems

### A Proof of Lemma 2: The covariance matrix $\mathbf{\Sigma_q}$ has rank $K-1$ in the Sharma-Song test

Proof. From Eq. (5), the covariance matrix $\mathbf{\Sigma_q}$ is equal to

$$\mathbf{\Sigma_q} = \mathbf{I} - \text{diag}(\mathbf{b})\mathbf{J}_K - \mathbf{J}_K\text{diag}(\mathbf{b}) + K\mathbf{b}\mathbf{b}^\top \tag{S1}$$

where $\mathbf{J}_K$ is a $K \times K$ matrix of all ones, $\mathbf{b}$ is a scaling vector $(b_1, \ldots, b_K)$ whose sum is one, and $\text{diag}(\mathbf{b})$ is a $K \times K$ matrix whose diagonal elements are $b_1, \ldots, b_K$ and off-diagonal elements are all zero. We can rewrite Eq. (5) as

$$\begin{aligned}
\mathbf{\Sigma_q} &= \mathbf{I} - \text{diag}(\mathbf{b})\mathbf{J}_K - \mathbf{J}_K\text{diag}(\mathbf{b}) + K\mathbf{b}\mathbf{b}^\top && \text{(S2)}\\
&= \mathbf{I} - \text{diag}(\mathbf{b})\mathbf{J}_K - \mathbf{J}_K\text{diag}(\mathbf{b}) + \text{diag}(\mathbf{b})\mathbf{J}_K\mathbf{J}_K\text{diag}(\mathbf{b}) \quad (\because \text{diag}(\mathbf{b})\mathbf{J}_K\mathbf{J}_K\text{diag}(\mathbf{b}) = K\mathbf{b}\mathbf{b}^\top) && \text{(S3)}\\
&= [\mathbf{I} - \text{diag}(\mathbf{b})\mathbf{J}_K][\mathbf{I} - \mathbf{J}_K\text{diag}(\mathbf{b})] && \text{(S4)}\\
&= [\mathbf{I} - \text{diag}(\mathbf{b})\mathbf{J}_K][\mathbf{I} - \text{diag}(\mathbf{b})\mathbf{J}_K]^\top && \text{(S5)}
\end{aligned}$$

A matrix $\mathbf{B}$ and its Gram matrix $\mathbf{B}\mathbf{B}^\top$ have the same rank $\text{rank}(\mathbf{B}\mathbf{B}^\top) = \text{rank}(\mathbf{B})$. Let $\mathbf{B} = \mathbf{I} - \text{diag}(\mathbf{b})\mathbf{J}_K$. Then we have $\mathbf{\Sigma_q} = \mathbf{B}\mathbf{B}^\top$ as apparently a Gram matrix, which must have the same rank with $\mathbf{B}$. Next, we show that the rank of $\mathbf{B}$ is $K-1$. We perform Gaussian elimination to transform matrix $\mathbf{B}$ to a row echelon form to obtain its rank. We can first write $\mathbf{B}$ as

$$\mathbf{B} = \mathbf{I} - \text{diag}(\mathbf{b})\mathbf{J}_K = \begin{bmatrix}
1-b_1 & -b_1 & -b_1 & \cdots & -b_1 & -b_1 \\
-b_2 & 1-b_2 & -b_2 & \cdots & -b_2 & -b_2 \\
-b_3 & -b_3 & 1-b_3 & \cdots & -b_3 & -b_3 \\
\vdots & \vdots & \vdots & \ddots & \vdots & \vdots \\
-b_{K-1} & -b_{K-1} & -b_{K-1} & \cdots & 1-b_{K-1} & -b_{K-1} \\
-b_K & -b_K & -b_K & \cdots & -b_K & 1-b_K
\end{bmatrix} \tag{S6}$$

Let $\mathbf{r}_i$ represent the elements on row $i$ in the matrix. Transforming row $i \neq K$ by

$$\mathbf{r}_i \to \mathbf{r}_i - \frac{b_i}{b_K}\mathbf{r}_K, \quad 1 \leq i \leq K-1 \tag{S7}$$

we obtain

$$\mathbf{B}_1 = \begin{bmatrix}
1 & 0 & 0 & \cdots & 0 & -b_1/b_K \\
0 & 1 & 0 & \cdots & 0 & -b_2/b_K \\
0 & 0 & 1 & \cdots & 0 & -b_3/b_K \\
\vdots & \vdots & \vdots & \ddots & \vdots & \vdots \\
0 & 0 & 0 & \cdots & 1 & -b_{K-1}/b_K \\
-b_K & -b_K & -b_K & \cdots & -b_K & 1-b_K
\end{bmatrix} \tag{S8}$$

If $b_K = 0$, we can always choose some row $k$ such that $b_k \neq 0$ instead of row $K$ to perform the row operations. Such a $k$ always exists provided that the sum of $b_1$ to $b_K$ is always one. For row $K$, we apply

$$\mathbf{r}_K \to \mathbf{r}_K + b_K \sum_{i=1}^{K-1} \mathbf{r}_i$$

on $\mathbf{B}_1$ to obtain

$$\mathbf{B}_2 = \begin{bmatrix}
1 & 0 & 0 & \cdots & 0 & -b_1/b_K \\
0 & 1 & 0 & \cdots & 0 & -b_2/b_K \\
0 & 0 & 1 & \cdots & 0 & -b_3/b_K \\
\vdots & \vdots & \vdots & \ddots & \vdots & \\
0 & 0 & 0 & \cdots & 1 & -b_{K-1}/b_K \\
0 & 0 & 0 & \cdots & 0 & 1-b_1-b_2-\cdots-b_K
\end{bmatrix} = \begin{bmatrix}
1 & 0 & 0 & \cdots & 0 & -b_1/b_K \\
0 & 1 & 0 & \cdots & 0 & -b_2/b_K \\
0 & 0 & 1 & \cdots & 0 & -b_3/b_K \\
\vdots & \vdots & \vdots & \ddots & \vdots & \\
0 & 0 & 0 & \cdots & 1 & -b_{K-1}/b_K \\
0 & 0 & 0 & \cdots & 0 & 0
\end{bmatrix} \quad (\because \sum_{i=1}^{K} b_i = 1) \tag{S9}$$

Since this row echelon form of matrix $\mathbf{B}$ has $K-1$ non-zero rows, the rank of $\mathbf{B} = \mathbf{I} - \text{diag}(\mathbf{b})\mathbf{J}_K$ must be $K-1$. Therefore, covariance matrix $\mathbf{\Sigma_q} = \mathbf{B}\mathbf{B}^\top$—the Gram matrix formed by $\mathbf{B}$—must also have the same rank of $K-1$.

## B Proof of Theorem 1: The Sharma-Song test statistic follows a chi-squared null distribution

Proof. The proof is based on the null hypothesis that the row and column variables in each $\mathbf{C}_k$ are independent and the $K$ tables are also independent of each other. By Helmert transform via Eqs. (1, 2, 3), the $r \times s$ contingency tables $\mathbf{C}_1, \ldots, \mathbf{C}_K$ give rise to matrices $\mathbf{E}_1, \ldots, \mathbf{E}_K$ all of dimension $r \times s$. Given the null hypothesis and by Lemma 1, elements in matrix $\mathbf{E}_k$ are i.i.d. standard normal $N(0,1)$ variables. Elements in $\mathbf{E}_k$ are also independent of those in $\mathbf{E}_l$ for $l \neq k$. When the row and column marginal distributions are calculated by sample marginal distributions, each $\mathbf{E}_k$ contains $M = (r-1)(s-1)$ elements of i.i.d. standard normal variables, excluding the first row and first column of all zeros (Lancaster, 1949). Indeed, sample marginal distributions are used in forming the Helmert matrices in the Sharma-Song test.

As $\mathbf{e}_k$ is a column-major vector representation of $\mathbf{E}_k$ without the first row or column, the $M$ components in $\mathbf{e}_k$ are i.i.d. standard normal variables. $\mathbf{e}_k$ and $\mathbf{e}_l$ are independent as $\mathbf{E}_k$ and $\mathbf{E}_l$ are independent when $k \neq l$. We obtain the pooled vector

$$\mathbf{e} = \sum_{k=1}^{K} \mathbf{e}_k \tag{S10}$$

Evidently, components in $\mathbf{e}$ are i.i.d. $N(0,K)$ (normal with zero mean and variance $K$). However, $\mathbf{e}$ is statistically dependent of $\mathbf{e}_k$. Let $e_{km}$ be the $m$-th component of $\mathbf{e}_k$. Let $e_m$ be the $m$-th component of $\mathbf{e}$. By Eq. (4), we can rewrite matrix $\mathbf{Q}$ by

$$\mathbf{Q} = \begin{bmatrix} \Delta_{11} & \Delta_{21} & \cdots & \Delta_{K1} \\ \Delta_{12} & \Delta_{22} & \cdots & \Delta_{K2} \\ \vdots & \vdots & \ddots & \vdots \\ \Delta_{1M} & \Delta_{2M} & \cdots & \Delta_{KM} \end{bmatrix} = \begin{bmatrix} e_{11} - b_1 e_1 & e_{21} - b_2 e_1 & \cdots & e_{K1} - b_K e_1 \\ e_{12} - b_1 e_2 & e_{22} - b_2 e_2 & \cdots & e_{K2} - b_K e_2 \\ \vdots & \vdots & \ddots & \vdots \\ e_{1M} - b_1 e_M & e_{2M} - b_2 e_M & \cdots & e_{KM} - b_K e_M \end{bmatrix} \tag{S11}$$

When all elements in $\mathbf{Q}$ are zero, the amount of 2nd-order differences in $\mathbf{C}_1, \ldots, \mathbf{C}_K$ is zero. So we ideally want to measure the null distribution of the distance from all elements to zero. As components within $\mathbf{e}_k$ are independent and components within $\mathbf{e}$ are independent, elements within each column of matrix $\mathbf{Q}$ are statistically independent, implying that the row vectors are statistically independent of each other. Components within each row are statistically dependent due to pooled vector $\mathbf{e}$ being dependent on all $\mathbf{e}_k$. As $\mathbf{q}_m$, row $m$ of $\mathbf{Q}$, is a linear combination of independent $N(0,1)$ variables, $\mathbf{q}_m$ follows a multivariate normal distribution $N(\mathbf{0}, \mathbf{\Sigma_q})$. We can derive its covariance matrix $\mathbf{\Sigma_q}$ as defined in Eq. (5). Equivalently,

$$\mathbf{\Sigma_q} = \mathbf{I} - \begin{bmatrix} b_1 + b_1 - b_1 b_1 K & b_2 + b_1 - b_2 b_1 K & \cdots & b_K + b_1 - b_K b_1 K \\ b_1 + b_2 - b_1 b_2 K & b_2 + b_2 - b_2 b_2 K & \cdots & b_K + b_2 - b_K b_2 K \\ \vdots & \vdots & \ddots & \vdots \\ b_1 + b_K - b_1 b_K K & b_2 + b_K - b_2 b_K K & \cdots & b_K + b_K - b_K b_K K \end{bmatrix} \tag{S12}$$

It is evident that the sum of column vectors of $\mathbf{\Sigma_q}$ is a zero vector $\mathbf{0}$. Thus, $\mathbf{\Sigma_q}$ is rank deficient without an inverse, implying that the Mahalanobis distance between $\mathbf{q}_m$ and $\mathbf{0}$ is undefined.

The projection step in the Sharma-Song test is essential in transforming $\mathbf{Q}$ to a collection of i.i.d. $N(0,1)$ variables to establish the chi-squared null distribution. We project each row vector $\mathbf{q}_m$ of $\mathbf{Q}$ by $\mathbf{z}_m = \mathbf{q}_m^\top \mathbf{S}_+$ to the column space of $\mathbf{\Sigma_q}$. $\mathbf{S}_+$ is spanned by eigenvectors corresponding to non-zero eigenvalues of $\mathbf{\Sigma_q}$. The eigenvalue decomposition of $\mathbf{\Sigma_q}$ is $\mathbf{S\Lambda S}^{-1}$. By the projection, $\mathbf{z}_m$ follows a multivariate normal $N(0, \mathbf{\Lambda}_+)$ distribution. $\mathbf{\Lambda}_+$ is a full-rank diagonal covariance matrix whose diagonal elements are non-zero eigenvalues of $\mathbf{\Sigma_q}$.

The squared Mahalanobis distance between $\mathbf{z}_m$ and the origin $\left\| \mathbf{q}_m^\top \mathbf{S}_+ \mathbf{\Lambda}_+^{-1/2} \right\|^2$ follows $\chi^2_{\text{rank}(\mathbf{\Sigma_q})}$, a chi-squared distribution with rank$(\mathbf{\Sigma_q})$ degrees of freedom (McLachlan, 1999). By Lemma 2, rank$(\mathbf{\Sigma_q}) = K - 1$. As the row vectors $\mathbf{q}_m$ $(m = 1, \ldots, M)$ in $\mathbf{Q}$ are independent of each other and have an equal covariance matrix $\mathbf{\Sigma_q}$, the Mahalanobis distances squared are i.i.d. $\chi^2_{K-1}$, that is

$$\left\| \mathbf{q}_1^\top \mathbf{S}_+ \mathbf{\Lambda}_+^{-1/2} \right\|^2, \quad \left\| \mathbf{q}_2^\top \mathbf{S}_+ \mathbf{\Lambda}_+^{-1/2} \right\|^2, \quad \ldots, \quad \left\| \mathbf{q}_M^\top \mathbf{S}_+ \mathbf{\Lambda}_+^{-1/2} \right\|^2 \sim \text{independently and identicially distributed } \chi^2_{K-1} \tag{S13}$$

Therefore the sum of these $M$ independent chi-squared statistics is also chi-squared, with degrees of freedom $(K-1) \cdot M = (K-1)(r-1)(s-1)$ being the sum of the degrees of freedom from each chi-squared statistic. As this sum is exactly the test statistic $D^2$ of the Sharma-Song test, we have just proven that $D^2$ asymptotically follows a chi-squared distribution with $\nu = (K-1)(r-1)(s-1)$ degrees of freedom

$$D^2 \sim \chi^2_{(K-1)(r-1)(s-1)} \tag{S14}$$

under the null hypothesis of the Sharma-Song test.

## C The Sharma-Song test algorithm

An algorithm to implement the Sharma-Song test is given as Algorithm S1 Sharma-Song-Test. The input to the algorithm is $K$ contingency tables of the same dimension. The output is the test statistic, the degrees of freedom, the effect size $\varepsilon$, and the $P$-value associated with the input tables for their 2nd-order differences.

**Algorithm S1** Sharma-Song-Test($\mathbf{C}_1, \ldots, \mathbf{C}_K$)

**for** $k = 1$ **to** $K$:
    Remove marginal effects from each $\mathbf{C}_k$ to get $\mathbf{A}_k$
    Perform both row- and column-Helmert transform: $\mathbf{E}_k = \mathbf{V}_k \mathbf{A}_k \mathbf{W}_k^\top$
    Vectorize $\mathbf{E}_k$ in column major excluding 1st row and 1st column to get $\mathbf{e}_k$
The pooled vector $\mathbf{e} = \mathbf{e}_1 + \cdots + \mathbf{e}_K$
Compute the scaling vector $\mathbf{b}$: $b_k = \sqrt{n_k} / \sum_{l=1}^{K} \sqrt{n_l}$
**for** $k = 1$ **to** $K$: Calculate deviation vectors $\mathbf{\Delta}_k$ as columns of matrix $\mathbf{Q}$
Calculate the covariance matrix $\mathbf{\Sigma_q}$
Perform eigenvalue decomposition on $\mathbf{\Sigma_q}$ to find its column space $\mathbf{S}_+$
Project rows of $\mathbf{Q}$ to $\mathbf{S}_+$
Calculate the sum of Mahalanobis distances squared $D^2$
Degrees of freedom $\nu = (K-1)(r-1)(s-1)$
$P$-value $=$ area under the upper tail of the chi-squared distribution $\chi^2_\nu$ greater than or equal to $D^2$
Calculate the effect size $\varepsilon = \sqrt{D^2/[n(r-1)(s-1)]}$, where $n = n_1 + \ldots + n_K$
**return** $D^2$, $\nu$, $P$-value, $\varepsilon$

## D The second-order network rewiring pipeline

To illustrate how to apply the Sharma-Song test to a mammalian transcriptome collection that contains samples from the ectoderm and primitive streak derived tissue types in mouse and human, we present a workflow diagram that includes all preprocessing and analysis steps as Figure S1. We assume the input data are already normalized and unwanted effects are removed. Our pipeline starts with removing unchanged genes occurring at the bottom $5\%$ median absolute deviation (MAD) in human and mouse data separately. We divide the samples of human and mouse data into four groups: human ectoderm, human primitive streak, mouse ectoderm, and mouse primitive streak. Genes with zero variance within each group are removed from further analysis. Selected genes go to next step for creating co-expression networks. We construct four comparisons: human ectoderm versus primitive streak, mouse ectoderm versus primitive streak, human versus mouse ectoderm, and human versus mouse primitive streak. In each comparison, all genes are discretized using an optimal univariate clustering algorithm (Wang and Song, 2011; Song and Zhong, 2020). For each comparison, we construct a co-expression network of all the conditions. Gene pairs represented in the form of contingency table are evaluated using Pearson's chi-squared test. We select significantly co-expressed patterns with Benjamini-Hochberg adjusted $P<0.1$ and Cramér's $V>0.8$ in at least one condition. Significantly co-expressed gene pairs are used to create a second-order rewired network. These gene pairs are scaled and shifted in their respective conditions. The scaled and shifted gene pairs are merged together and discretized to form contingency tables. The gene pairs represented by contingency tables are evaluated by Sharma-Song test to build a second-order rewired network. We further obtain $\varepsilon_{60}$, the effect size cutoff at a statistical power of 60% depending on the maximum table size obtained among all the comparison. We select significant second-order differential patterns with Benjamini-Hochberg adjusted $P<0.05$ and $\varepsilon>\varepsilon_{60}$ for all comparisons. We provide an R package 'DiffXCoExpNet' which can compare two or more experimental conditions of an omic dataset and generate a second-order rewired network. We have provided the R script files and a vignette to guide the user to perform a second-order rewired analysis through the pipeline.

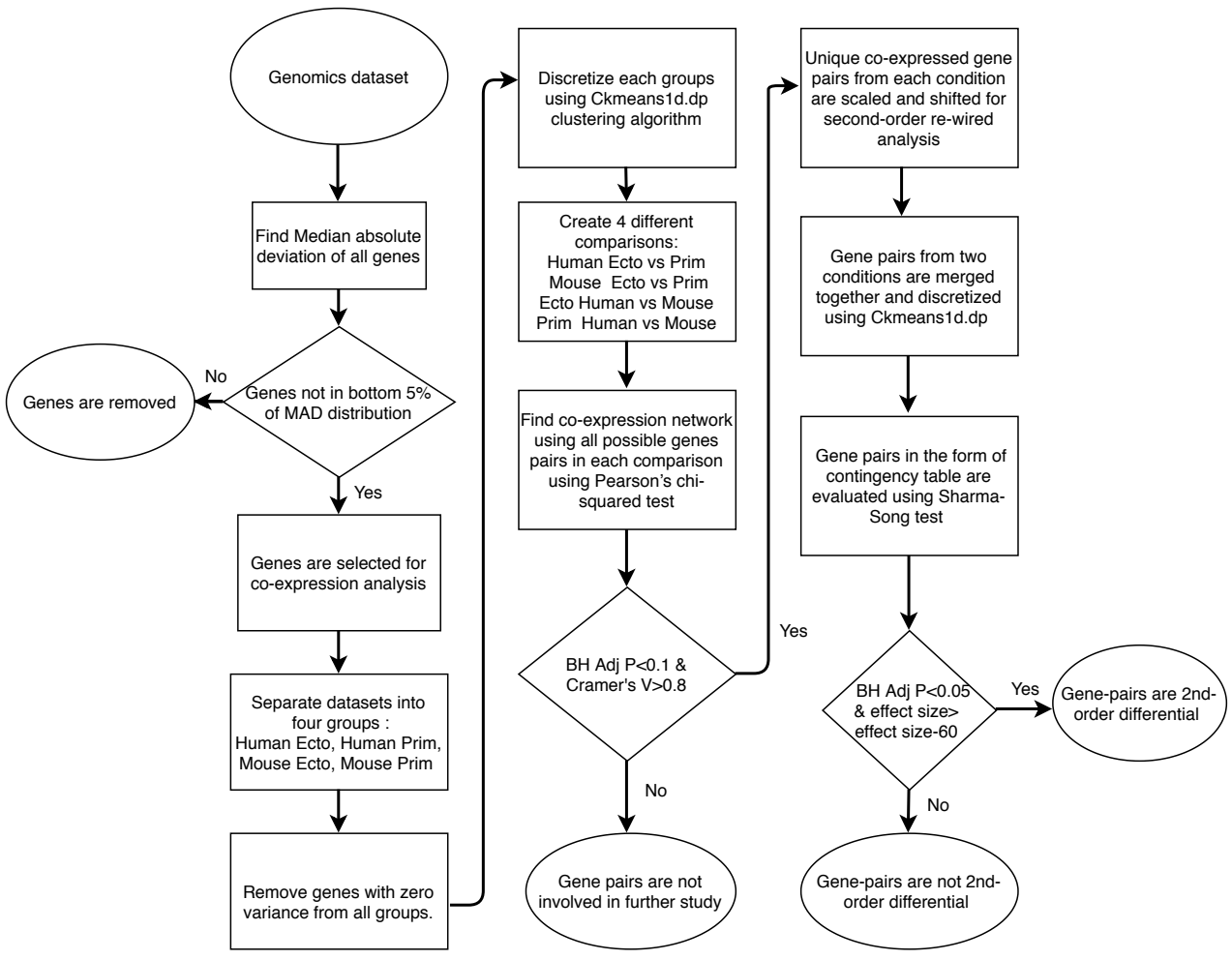


**Fig. S1.** A workflow used in the pipeline of second-order network rewiring analysis. The input data contain samples from within and between ectoderm and primitive streak derived tissue groups of human and mouse. We assume the input data are properly normalized and log-transformed. We start with finding high dynamic genes after removing low median absolute deviation (MAD) genes. FANOTM5, Evo-devo and Yang et al. datasets were divided into four species-tissue groups for further analysis. Genes with zero variance are removed from all four groups and then discretized. Within each group, a co-expression network is created for each condition under comparison. Significant unique co-expressed gene pairs are scaled and shifted. Then all selected gene pairs are evaluated by the Sharma-Song test for detecting second-order rewiring. Gene patterns with BH adjusted $P$-value $< 0.05$ and effect size $\varepsilon>\varepsilon_{60}$ are declared as second-order differential patterns. BH stands for the Benjamini-Hochberg multiple testing correction.

## E High-degree hub genes in second-order rewired networks during mammalian development

To examine whether the 2nd-order rewired gene networks during mammalian development are reproducible, we examined hub genes in the rewired networks derived from the FANTOM5, Evo-devo, and Yang et al. data collections. We observe that common high-degree hub genes are more prominent in highly 2nd-order differential patterns between the Evo-devo and Yang et al. collections. We define the node degree of a hub gene as the number of 2nd-order differential interactions involving the hub gene. After sorting all 2nd-order differential interactions by increasing $p$-value, we partitioned the interactions into five equal percentile groups: 0–20%, 20–40%, 40–60%, 60–80%, 80–100%. The 0–20% percentile group contains the strongest 2nd-order differential gene interactions. Within each percentile group, we tabulated numbers of genes with degrees 1 to 100. Then we obtained the number of common hub genes between two collections for each degree. For each of the four comparisons (human ectoderm vs primitive streak, mouse ectoderm vs primitive streak, human vs mouse ectoderm and human vs mouse primitive streak), we generated curves showing the number of common hub genes across the five percentile groups at each degree from 1 to 100, as shown in Figure S2. We observe that the strongest 2nd-order differential percentile group (0-20%) contain the largest numbers of common high-degree hub genes between collections in all four comparisons. Although the low-degree genes are more often shared across collections, their corresponding curves are flat across percentile groups, irrespective of the strength of 2nd-order rewiring. Therefore, we consider the common high-degree hub genes a reproducible feature of the 2nd-order rewired gene networks.

The FANTOM5 collection does not overlap with the other two collections in terms of common hub genes, due to several possible reasons. First, FANTOM5 data used in this study have a relatively small sample size, thus leading to a relatively low statistical power in contrast to the other two collections. Second, FANTOM5 measured expression of transcription start sites of genes, different from the other two collections measuring all transcript reads within a gene. Third, the CAGE technology used in FANTOM5 is different from the RNA-seq technology used for the other two collections. It will have to be resolved in the future when other large sample sized studies of mammalian development become available.

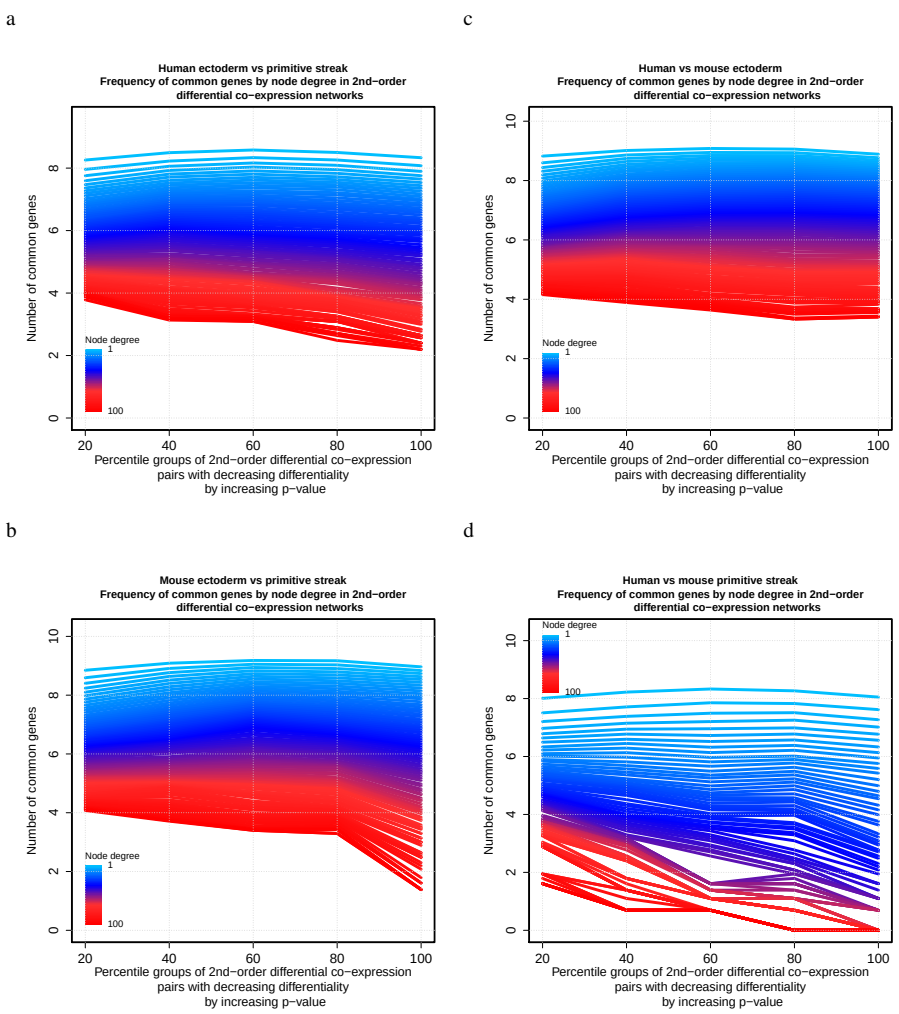


**Fig. S2. Number of common hub genes in 2nd-order differential co-expression networks between Evo-devo and Yang et al. collections by differentiality percentile group and node degree.** Each line represents the number of common genes at a given node degree across five percentile groups of 2nd-order differential interactions ordered by increasing $p$-value. The color spectrum from blue to red represents node degree from 1 to 100. The curves shows that the number of common high-degree hub genes decreases as 2nd-order differentiality becomes weaker across the groups. Results are shown for four comparisons: **(a)** human ectoderm versus primitive streak, **(b)** mouse ectoderm versus primitive streak, **(c)** human vs mouse ectoderm, and **(d)** human versus mouse primitive streak.

## F Reproducible second-order rewired gene-gene patterns during mammalian development

Here, we report second-order differential gene pairs found for each species-tissue group comparison that are common to all three mammalian developmental transcriptome datasets of FANTOM5, Evo-devo and Yang et al. For each comparison, we found common co-expressed second-order differential patterns obtained using above pipeline among all datasets. We obtained 55 reproducible second-order rewired gene pairs between human ectoderm and primitive streak derived tissue types, 241 reproducible second-order rewired gene pairs between mouse ectoderm and primitive streak derived tissue types, 57 reproducible second-order rewired gene pairs between human and mouse primitive streak derived tissue types and 85 reproducible second-order rewired gene pairs between human and mouse ectoderm derived tissue types. We observed same mechanistic rewiring in some of these reproducible patterns among all datasets. Reproducible 2nd-order rewired gene pairs are shown for each of the four comparisons among the species-tissue groups in Tables S1, S2, S3, and S4.

Table S1: A total of 55 reproducible second-order rewired gene pairs between human ectoderm and primitive streak derived tissue types. Gene pairs with their second-order differential $P$-values and effect sizes $\varepsilon$ are shown as obtained from FANTOM5, Yang et al. and Evo-devo datasets, respectively.

| **Gene** | **Gene** | **FANTOM5** | **Yang el al.** | **Evo-devo** |
|---|---|---|---|---|
| | | $P$-value / Effect size $\varepsilon$ | $P$-value / Effect size $\varepsilon$ | $P$-value / Effect size $\varepsilon$ |
| ATP8B2 | SLC35F1 | 0.0103 / 0.60 | 0.0027 / 0.41 | 2e-11 / 0.3 |
| ABLIM1 | PKIB | 0.0307 / 0.47 | 0.00033 / 0.49 | 3.4e-24 / 0.62 |
| TIAM1 | MPP3 | 0.0319 / 0.47 | 0.0019 / 0.42 | 1.1e-15 / 0.35 |
| PTGFRN | MPP3 | 0.0162 / 0.54 | 0.00035 / 0.49 | 1.7e-19 / 0.4 |
| CHN2 | CDR2L | 0.0204 / 0.52 | 8.3e-06 / 0.64 | 1.4e-12 / 0.42 |
| TMSB10 | KCTD2 | 0.0146 / 0.55 | 7.2e-05 / 0.55 | 7.4e-12 / 0.3 |
| LONRF3 | KCTD2 | 0.0121 / 0.57 | 1.5e-06 / 0.7 | 2e-22 / 0.43 |
| RNF128 | GALK1 | 0.0066 / 0.70 | 0.00014 / 0.52 | 8.8e-18 / 0.38 |
| ST6GALNAC5 | STK10 | 0.0113 / 0.59 | 0.0011 / 0.45 | 9.1e-06 / 0.26 |
| PPP1R3C | ENO3 | 0.0083 / 0.64 | 0.00031 / 0.49 | 6.6e-22 / 0.58 |
| AFAP1L2 | ALDOC | 0.0168 / 0.54 | 8.7e-05 / 0.54 | 1.2e-20 / 0.41 |
| VANGL2 | ALDOC | 0.0234 / 0.50 | 1.3e-06 / 0.71 | 1.3e-12 / 0.31 |
| DOK7 | RNF43 | 0.0286 / 0.48 | 0.00042 / 0.48 | 7.5e-13 / 0.32 |
| CCDC88B | NLN | 0.0252 / 0.49 | 0.014 / 0.33 | 1.3e-11 / 0.3 |
| NDFIP2 | RGS14 | 0.0348 / 0.46 | 0.0012 / 0.44 | 3.5e-08 / 0.33 |
| NRGN | RGS14 | 0.0254 / 0.49 | 3e-04 / 0.5 | 7.5e-07 / 0.29 |
| XYLB | FBP1 | 0.0089 / 0.63 | 0.0012 / 0.44 | 1.6e-12 / 0.26 |
| HPN | GLUD1 | 0.0091 / 0.62 | 0.00013 / 0.53 | 6.2e-15 / 0.29 |
| RAP1GAP | PHYHIP | 0.0055 / 0.78 | 0.0081 / 0.36 | 1.5e-10 / 0.38 |
| GPR155 | NIPAL2 | 0.0105 / 0.60 | 0.0014 / 0.44 | 6.4e-09 / 0.35 |
| LETM2 | RGS22 | 0.0078 / 0.65 | 0.00096 / 0.45 | 4.2e-09 / 0.26 |
| CPT1B | TMEM65 | 0.0283 / 0.48 | 0.00053 / 0.47 | 1e-13 / 0.45 |
| ARNT2 | RND1 | 0.0216 / 0.51 | 1.1e-05 / 0.62 | 8.9e-24 / 0.44 |
| KCTD14 | SOCS1 | 0.0235 / 0.50 | 0.00048 / 0.48 | 4.9e-06 / 0.27 |
| MICAL2 | CHRD | 0.0146 / 0.55 | 0.0012 / 0.44 | 2.5e-15 / 0.48 |
| SORCS1 | ST6GAL1 | 0.0146 / 0.55 | 1.9e-05 / 0.6 | 1.4e-08 / 0.25 |
| SH3RF1 | ST6GAL1 | 0.0073 / 0.67 | 2.6e-05 / 0.59 | 4.1e-15 / 0.26 |
| WSCD2 | BDH1 | 0.0315 / 0.47 | 5.8e-06 / 0.65 | 8.8e-20 / 0.4 |
| EZR | TIAM1 | 0.0207 / 0.51 | 0.00011 / 0.53 | 1.1e-15 / 0.48 |
| P2RX4 | TIAM1 | 0.0224 / 0.51 | 0.013 / 0.34 | 9.2e-24 / 0.61 |
| LPCAT3 | TIAM1 | 0.0243 / 0.50 | 0.0012 / 0.44 | 7.5e-30 / 0.69 |
| TMSB10 | TIAM1 | 0.0246 / 0.49 | 0.00031 / 0.49 | 2e-16 / 0.49 |
| LONRF3 | TIAM1 | 0.0283 / 0.48 | 0.00052 / 0.47 | 1.1e-21 / 0.58 |
| POLB | TRIM36 | 0.0235 / 0.50 | 4.6e-05 / 0.57 | 2.5e-17 / 0.31 |
| ALS2 | ISOC1 | 0.0110 / 0.59 | 0.0012 / 0.44 | 6e-21 / 0.34 |
| MPZL3 | CCDC88B | 0.0252 / 0.49 | 0.0088 / 0.36 | 9.8e-10 / 0.37 |
| TACC1 | MDK | 0.0140 / 0.56 | 0.00085 / 0.46 | 1.9e-07 / 0.31 |
| LETM2 | ZMYND12 | 0.0307 / 0.47 | 9.4e-05 / 0.54 | 8.7e-07 / 0.29 |
| S1PR5 | MARCKSL1 | 0.0336 / 0.46 | 0.0051 / 0.38 | 8.8e-12 / 0.3 |
| POLB | P2RX4 | 0.0113 / 0.59 | 0.0036 / 0.4 | 1.1e-20 / 0.56 |
| CACNA1A | P2RX4 | 0.0174 / 0.53 | 0.0027 / 0.41 | 9.4e-23 / 0.36 |
| CACNA1A | TMSB10 | 0.0146 / 0.55 | 6e-04 / 0.47 | 5.4e-13 / 0.27 |
| POLB | EEF2K | 0.0246 / 0.49 | 0.0031 / 0.4 | 2.3e-19 / 0.39 |
| COIL | PCSK4 | 0.0243 / 0.50 | 0.0019 / 0.42 | 4.6e-18 / 0.28 |
| MYCBPAP | PCSK4 | 0.0060 / 0.72 | 0.00093 / 0.45 | 2.4e-19 / 0.29 |
| COIL | IZUMO4 | 0.0324 / 0.47 | 0.00059 / 0.47 | 1.5e-13 / 0.33 |
| OTUB2 | IZUMO4 | 0.0269 / 0.49 | 0.0021 / 0.42 | 9.1e-14 / 0.33 |
| BRAP | IZUMO4 | 0.0269 / 0.49 | 0.00016 / 0.52 | 9.2e-15 / 0.34 |
| COIL | ZFR2 | 0.0161 / 0.54 | 0.001 / 0.45 | 9.8e-15 / 0.25 |
| ACRBP | ZFR2 | 0.0323 / 0.47 | 9e-06 / 0.63 | 3.9e-12 / 0.31 |
| CCDC87 | COIL | 0.0234 / 0.50 | 0.0018 / 0.43 | 5e-15 / 0.26 |
| FAM71E1 | COIL | 0.0140 / 0.56 | 0.00078 / 0.46 | 4.2e-10 / 0.28 |
| KDM4D | OTUB2 | 0.0083 / 0.64 | 0.00011 / 0.54 | 1.1e-09 / 0.27 |
| SH3RF1 | ANKS6 | 0.0144 / 0.56 | 5.7e-05 / 0.56 | 2.9e-16 / 0.36 |
| LRWD1 | BRAP | 0.0198 / 0.52 | 0.00018 / 0.52 | 1.4e-12 / 0.31 |
| KDM4D | BRAP | 0.0083 / 0.64 | 0.0041 / 0.39 | 1.6e-09 / 0.27 |
| MMD2 | LRWD1 | 0.0171 / 0.53 | 0.00019 / 0.51 | 3.6e-13 / 0.27 |
| AGBL5 | LRWD1 | 0.0094 / 0.62 | 0.0061 / 0.37 | 1.7e-18 / 0.39 |
| KDM4D | FAM71E1 | 0.0234 / 0.50 | 0.0019 / 0.42 | 1.1e-12 / 0.43 |

Table S2: A total of 241 reproducible second-order rewired gene pairs between mouse ectoderm and primitive streak derived tissue types. Gene pairs with their second-order differential $P$-values and effect sizes $\varepsilon$ are shown as obtained from FANTOM5, Yang et al. and Evo-devo datasets, respectively.

| **Gene** | **Gene** | **FANTOM5** | **Yang el al.** | **Evo-devo** |
|---|---|---|---|---|
| | | $P$-value / Effect size $\varepsilon$ | $P$-value / Effect size $\varepsilon$ | $P$-value / Effect size $\varepsilon$ |
| Megf11 | Lin7a | 0.0108 / 0.65 | 0.0023 / 0.58 | 3.3e-15 / 0.28 |
| Ttll7 | Tbk1 | 0.0261 / 0.49 | 0.013 / 0.45 | 1.3e-09 / 0.26 |
| Bphl | Avpr1a | 0.0260 / 0.49 | 0.05 / 0.35 | 2.6e-15 / 0.34 |
| Kctd17 | B4galnt1 | 0.0233 / 0.51 | 0.017 / 0.43 | 1.6e-13 / 0.26 |
| Als2 | Itga7 | 0.0195 / 0.53 | 0.0044 / 0.52 | 1.9e-19 / 0.38 |
| Slco4a1 | Itga7 | 0.0134 / 0.58 | 0.024 / 0.41 | 1e-17 / 0.36 |
| Eml1 | Lama4 | 0.0188 / 0.53 | 0.0038 / 0.53 | 5.1e-31 / 0.3 |
| Nxn | Slc16a10 | 0.0122 / 0.61 | 0.0016 / 0.62 | 1.1e-30 / 0.4 |
| Reep6 | Prmt2 | 0.0302 / 0.48 | 0.041 / 0.37 | 1.1e-08 / 0.33 |
| Ror1 | Prmt2 | 0.0146 / 0.58 | 0.0075 / 0.48 | 1.2e-13 / 0.43 |
| Wdr81 | Dip2a | 0.0148 / 0.58 | 0.046 / 0.36 | 3.1e-17 / 0.3 |
| Ulk4 | Pcsk4 | 0.0260 / 0.49 | 0.0094 / 0.47 | 8.3e-15 / 0.28 |
| Fnbp1 | Ascl1 | 0.0184 / 0.54 | 0.027 / 0.4 | 2.6e-13 / 0.26 |
| Diras2 | Apaf1 | 0.0269 / 0.49 | 0.00099 / 0.68 | 2.5e-09 / 0.34 |
| B3galnt1 | Fzd2 | 0.0233 / 0.51 | 0.029 / 0.39 | 3.7e-22 / 0.56 |
| Cerk | Fads6 | 0.0125 / 0.61 | 0.00082 / 0.7 | 8.2e-17 / 0.3 |
| Rfx2 | Mafg | 0.0134 / 0.58 | 0.0046 / 0.51 | 3.8e-13 / 0.31 |
| Lin54 | Fn3k | 0.0206 / 0.52 | 0.038 / 0.37 | 1.2e-22 / 0.34 |
| Slc9a3 | Stk10 | 0.0155 / 0.56 | 0.007 / 0.49 | 9.3e-13 / 0.26 |
| Bmp1 | Stk10 | 0.0261 / 0.49 | 0.025 / 0.4 | 1.6e-12 / 0.3 |
| Exph5 | Stk10 | 0.0250 / 0.50 | 0.0094 / 0.47 | 9e-12 / 0.29 |
| Iqgap2 | Dusp18 | 0.0190 / 0.53 | 0.00097 / 0.68 | 2.6e-14 / 0.44 |
| Ttc7b | Mtfp1 | 0.0173 / 0.55 | 0.039 / 0.37 | 1.2e-08 / 0.33 |
| Marveld2 | Ccdc69 | 0.0097 / 0.72 | 0.026 / 0.4 | 1.6e-16 / 0.35 |
| Npm3 | Tnfaip1 | 0.0251 / 0.50 | 0.015 / 0.44 | 8.9e-12 / 0.29 |
| Stam2 | Prr11 | 0.0237 / 0.50 | 0.03 / 0.39 | 2.7e-09 / 0.34 |
| Sh3bp4 | Cuedc1 | 0.0113 / 0.63 | 0.02 / 0.42 | 2.3e-10 / 0.37 |
| Slc14a1 | Ttc7b | 0.0178 / 0.54 | 0.004 / 0.53 | 1.1e-19 / 0.32 |
| Stk17b | Slc9a3 | 0.0206 / 0.52 | 0.011 / 0.45 | 1.1e-15 / 0.28 |
| Evc2 | Iqgap2 | 0.0151 / 0.57 | 0.0084 / 0.47 | 9.1e-22 / 0.34 |
| Glb1l2 | Fam107a | 0.0097 / 0.76 | 0.041 / 0.37 | 1e-18 / 0.31 |
| Stap2 | Itgb7 | 0.0378 / 0.46 | 0.027 / 0.4 | 5.1e-17 / 0.26 |
| Rbpms | Map3k12 | 0.0260 / 0.50 | 0.0032 / 0.54 | 7.6e-15 / 0.28 |
| Fgf7 | Khdrbs3 | 0.0343 / 0.47 | 0.0034 / 0.54 | 1.5e-21 / 0.4 |
| Pxn | Khdrbs3 | 0.0151 / 0.57 | 0.028 / 0.4 | 4.5e-16 / 0.34 |
| Tll1 | Khdrbs3 | 0.0177 / 0.54 | 0.0034 / 0.54 | 1.8e-20 / 0.39 |
| Exph5 | Khdrbs3 | 0.0260 / 0.49 | 0.022 / 0.41 | 2.9e-21 / 0.29 |
| Stat4 | Chrac1 | 0.0221 / 0.51 | 0.015 / 0.44 | 8.9e-21 / 0.29 |
| Sema7a | Grina | 0.0325 / 0.47 | 0.0037 / 0.53 | 8.1e-14 / 0.43 |
| St6galnac6 | Mgat3 | 0.0122 / 0.61 | 0.029 / 0.39 | 7.4e-28 / 0.28 |
| Rnd3 | Fgf12 | 0.0325 / 0.47 | 0.0068 / 0.49 | 2.1e-19 / 0.52 |
| Cdon | Tmem44 | 0.0162 / 0.56 | 0.002 / 0.59 | 1.5e-11 / 0.29 |
| Chst10 | Hagh | 0.0119 / 0.62 | 0.019 / 0.42 | 1.3e-14 / 0.27 |
| Stk17b | Stap2 | 0.0268 / 0.49 | 0.0061 / 0.49 | 7.3e-11 / 0.28 |
| Ahcyl1 | Arhgap28 | 0.0113 / 0.64 | 0.024 / 0.41 | 1.2e-09 / 0.35 |
| Kifap3 | Ltbp1 | 0.0097 / 0.73 | 0.031 / 0.39 | 5.6e-27 / 0.28 |
| Etfb | Cdca5 | 0.0122 / 0.61 | 0.024 / 0.41 | 1.2e-13 / 0.32 |
| Chmp4b | Prdx5 | 0.0214 / 0.51 | 0.013 / 0.44 | 4.5e-10 / 0.36 |
| Lonrf2 | Prrx1 | 0.0195 / 0.53 | 0.024 / 0.4 | 5.7e-24 / 0.36 |
| Slc4a3 | Prrx1 | 0.0236 / 0.51 | 0.0031 / 0.55 | 6.3e-21 / 0.33 |
| Amotl2 | Mcm3 | 0.0188 / 0.53 | 0.018 / 0.43 | 3.1e-12 / 0.3 |
| Exph5 | Stk17b | 0.0260 / 0.49 | 0.0026 / 0.56 | 2.1e-14 / 0.32 |
| Megf11 | Als2 | 0.0168 / 0.55 | 0.015 / 0.44 | 5.6e-21 / 0.55 |
| Arhgap33 | Pak6 | 0.0333 / 0.47 | 0.0077 / 0.48 | 4.1e-10 / 0.36 |
| Stam2 | Nusap1 | 0.0237 / 0.50 | 0.0075 / 0.48 | 9.9e-17 / 0.35 |
| Inpp5a | Shf | 0.0115 / 0.63 | 0.03 / 0.39 | 7.8e-15 / 0.33 |
| Snapin | Xrn2 | 0.0361 / 0.46 | 0.0019 / 0.61 | 5.6e-07 / 0.29 |
| Casq2 | Slco4a1 | 0.0184 / 0.54 | 0.0046 / 0.52 | 9.3e-16 / 0.34 |
| Ptgfr | Osbpl6 | 0.0279 / 0.49 | 0.046 / 0.36 | 1e-09 / 0.26 |
| Bnc2 | Mapk8ip1 | 0.0106 / 0.65 | 0.013 / 0.45 | 1.6e-10 / 0.27 |
| Vamp8 | Spata6 | 0.0134 / 0.60 | 0.004 / 0.53 | 2.7e-12 / 0.25 |

| | | | | |
|---|---|---|---|---|
| Reln | Pik3r3 | 0.0173 / 0.55 | 0.016 / 0.43 | 1.6e-13 / 0.26 |
| Rps5 | Prkcz | 0.0206 / 0.52 | 0.0032 / 0.55 | 6.1e-16 / 0.29 |
| Pgm2l1 | Mcm7 | 0.0098 / 0.69 | 0.018 / 0.43 | 1.4e-21 / 0.4 |
| Yipf2 | Gpr146 | 0.0281 / 0.49 | 0.025 / 0.4 | 3.6e-08 / 0.32 |
| Cx3cl1 | Ctbp2 | 0.0134 / 0.59 | 0.0052 / 0.51 | 3e-21 / 0.33 |
| Fam98c | Pwwp2b | 0.0132 / 0.60 | 0.046 / 0.36 | 3.2e-19 / 0.38 |
| Clmn | Zbtb39 | 0.0314 / 0.48 | 0.034 / 0.38 | 1.1e-06 / 0.28 |
| Sfxn2 | Pcbd1 | 0.0113 / 0.63 | 0.02 / 0.42 | 3.2e-16 / 0.29 |
| Atxn3 | Pcsk4 | 0.0206 / 0.52 | 0.029 / 0.39 | 4.9e-25 / 0.27 |
| Nphp1 | Mex3d | 0.0206 / 0.52 | 0.018 / 0.42 | 5.6e-10 / 0.27 |
| Rnf32 | Mex3d | 0.0260 / 0.49 | 0.042 / 0.37 | 5.4e-10 / 0.27 |
| Odf2 | Psmc3ip | 0.0206 / 0.52 | 0.015 / 0.44 | 1.6e-14 / 0.27 |
| Ttc21b | Wdpcp | 0.0206 / 0.52 | 0.0027 / 0.56 | 1.1e-16 / 0.26 |
| Shroom1 | Sec24a | 0.0223 / 0.51 | 0.0023 / 0.58 | 1.6e-16 / 0.48 |
| Itgal | Myo1g | 0.0260 / 0.49 | 0.0059 / 0.5 | 6.1e-17 / 0.35 |
| Upf3a | Ap2b1 | 0.0260 / 0.49 | 0.049 / 0.36 | 1.3e-14 / 0.33 |
| Rasl11a | Tbx2 | 0.0165 / 0.55 | 0.004 / 0.53 | 1.7e-20 / 0.33 |
| Clip2 | Itga3 | 0.0149 / 0.57 | 0.048 / 0.36 | 6.8e-08 / 0.31 |
| Ccnk | Lrrc46 | 0.0206 / 0.52 | 0.019 / 0.42 | 7.2e-14 / 0.27 |
| Acrbp | Atxn3 | 0.0349 / 0.47 | 0.0048 / 0.51 | 1.3e-14 / 0.33 |
| Fam118b | Atxn3 | 0.0206 / 0.52 | 0.0048 / 0.51 | 2.8e-20 / 0.29 |
| Ctsa | Ddx24 | 0.0240 / 0.50 | 0.029 / 0.39 | 6e-13 / 0.31 |
| Nkapl | Ccnk | 0.0260 / 0.49 | 0.0041 / 0.52 | 7.2e-14 / 0.27 |
| Cep72 | Ccnk | 0.0260 / 0.49 | 0.009 / 0.47 | 5.7e-10 / 0.27 |
| Phf7 | Ccnk | 0.0260 / 0.49 | 0.019 / 0.42 | 9.3e-13 / 0.41 |
| Ddhd1 | Ccnk | 0.0260 / 0.49 | 0.0071 / 0.48 | 7.2e-14 / 0.27 |
| Ropn1l | Ccnk | 0.0260 / 0.49 | 0.0041 / 0.52 | 7.5e-12 / 0.29 |
| Chrac1 | Ccnk | 0.0260 / 0.49 | 0.0076 / 0.48 | 1.3e-14 / 0.33 |
| Ypel1 | Ccnk | 0.0206 / 0.52 | 0.032 / 0.39 | 1.3e-14 / 0.33 |
| Tctex1d2 | Ccnk | 0.0260 / 0.49 | 0.0016 / 0.62 | 1.3e-14 / 0.33 |
| Lca5l | Ccnk | 0.0260 / 0.49 | 0.0041 / 0.52 | 7.2e-14 / 0.27 |
| Efhb | Ccnk | 0.0260 / 0.49 | 0.0041 / 0.52 | 7.2e-14 / 0.27 |
| Cabyr | Ccnk | 0.0260 / 0.49 | 0.0019 / 0.59 | 7.2e-14 / 0.27 |
| Spata24 | Ccnk | 0.0260 / 0.49 | 0.019 / 0.42 | 7.2e-14 / 0.27 |
| Ccdc87 | Ccnk | 0.0206 / 0.52 | 0.045 / 0.36 | 7.2e-14 / 0.27 |
| Spata17 | Ccnk | 0.0177 / 0.54 | 0.045 / 0.36 | 7.2e-14 / 0.27 |
| Ppp1r42 | Ccnk | 0.0260 / 0.49 | 0.0041 / 0.52 | 7.2e-14 / 0.27 |
| Nphp1 | Ccnk | 0.0206 / 0.52 | 0.0015 / 0.62 | 7.5e-11 / 0.38 |
| Kif3b | Ccnk | 0.0260 / 0.49 | 0.0022 / 0.58 | 7.2e-14 / 0.27 |
| Wfdc3 | Ccnk | 0.0260 / 0.49 | 0.0076 / 0.48 | 1.3e-14 / 0.33 |
| Ddx20 | Ccnk | 0.0206 / 0.52 | 0.012 / 0.45 | 1.3e-14 / 0.33 |
| Lrriq3 | Ccnk | 0.0260 / 0.49 | 0.0019 / 0.59 | 1.3e-14 / 0.33 |
| Lrrc34 | Ccnk | 0.0260 / 0.49 | 0.0026 / 0.56 | 1.3e-14 / 0.33 |
| Sclt1 | Ccnk | 0.0206 / 0.52 | 0.0042 / 0.52 | 1.5e-15 / 0.46 |
| Fhad1 | Ccnk | 0.0260 / 0.49 | 0.0042 / 0.52 | 1.5e-15 / 0.46 |
| Aptx | Ccnk | 0.0177 / 0.54 | 0.045 / 0.36 | 7.5e-12 / 0.29 |
| Wdr31 | Ccnk | 0.0206 / 0.52 | 0.0019 / 0.59 | 1.3e-14 / 0.33 |
| Iqce | Ccnk | 0.0260 / 0.49 | 0.0029 / 0.55 | 1.3e-14 / 0.33 |
| Rnf32 | Ccnk | 0.0260 / 0.49 | 0.019 / 0.42 | 7.5e-11 / 0.38 |
| Ccdc96 | Ccnk | 0.0260 / 0.49 | 0.0026 / 0.56 | 7.2e-14 / 0.27 |
| Amn1 | Ccnk | 0.0260 / 0.49 | 0.046 / 0.36 | 1.3e-14 / 0.33 |
| Fank1 | Ccnk | 0.0206 / 0.52 | 0.0026 / 0.56 | 7.2e-14 / 0.27 |
| Wdr93 | Ccnk | 0.0260 / 0.49 | 0.009 / 0.47 | 7.5e-12 / 0.29 |
| Ankrd42 | Ccnk | 0.0260 / 0.49 | 0.0026 / 0.56 | 1.5e-15 / 0.46 |
| Txnl4b | Ccnk | 0.0260 / 0.49 | 0.045 / 0.36 | 1.3e-14 / 0.33 |
| Polb | Ccnk | 0.0260 / 0.49 | 0.0029 / 0.55 | 7.2e-14 / 0.27 |
| Lrp2bp | Ccnk | 0.0260 / 0.49 | 0.045 / 0.36 | 1.3e-14 / 0.33 |
| Kdm4d | Ccnk | 0.0260 / 0.49 | 0.0026 / 0.56 | 7.2e-14 / 0.27 |
| Fam118b | Ccnk | 0.0260 / 0.49 | 0.019 / 0.42 | 1.3e-14 / 0.33 |
| Spa17 | Ccnk | 0.0260 / 0.49 | 0.034 / 0.38 | 1.3e-14 / 0.33 |
| Efhc2 | Ccnk | 0.0260 / 0.49 | 0.0026 / 0.56 | 1.3e-14 / 0.33 |
| Ttc21b | Hspa2 | 0.0260 / 0.49 | 0.0066 / 0.49 | 3.7e-23 / 0.26 |
| Ttc21b | Wdr35 | 0.0260 / 0.49 | 0.0059 / 0.5 | 1.4e-24 / 0.32 |
| Pomt1 | Zc3h14 | 0.0206 / 0.52 | 0.037 / 0.38 | 1.4e-12 / 0.25 |
| Sh3gl3 | Pik3r1 | 0.0206 / 0.52 | 0.0042 / 0.52 | 9.5e-19 / 0.37 |
| Ulk4 | Nkapl | 0.0260 / 0.49 | 0.0089 / 0.47 | 7.9e-16 / 0.29 |
| Pter | Bphl | 0.0206 / 0.52 | 0.0025 / 0.57 | 2.4e-12 / 0.41 |
| Upf3a | Cep72 | 0.0260 / 0.49 | 0.034 / 0.38 | 5.7e-10 / 0.27 |

| | | | | |
|---|---|---|---|---|
| Polb | Cep72 | 0.0260 / 0.49 | 0.034 / 0.38 | 1.9e-25 / 0.27 |
| Ccdc87 | Phf7 | 0.0206 / 0.52 | 0.011 / 0.46 | 1.7e-12 / 0.25 |
| Xkr8 | Phf7 | 0.0206 / 0.52 | 0.0029 / 0.55 | 7.1e-12 / 0.29 |
| Upf3a | Phf7 | 0.0260 / 0.49 | 0.004 / 0.53 | 9.3e-13 / 0.41 |
| Fam118b | Phf7 | 0.0260 / 0.49 | 0.035 / 0.38 | 7.1e-12 / 0.29 |
| Ddx20 | Ddhd1 | 0.0206 / 0.52 | 0.04 / 0.37 | 7.2e-29 / 0.29 |
| Lyar | Ddhd1 | 0.0260 / 0.49 | 0.026 / 0.4 | 2e-30 / 0.3 |
| Ulk4 | Ddhd1 | 0.0260 / 0.49 | 0.016 / 0.43 | 1.4e-19 / 0.32 |
| Ribc1 | Ddhd1 | 0.0206 / 0.52 | 0.014 / 0.44 | 4e-22 / 0.25 |
| Upf3a | Ropn1l | 0.0260 / 0.49 | 0.0088 / 0.47 | 7.5e-12 / 0.29 |
| Amotl2 | Racgap1 | 0.0373 / 0.46 | 0.011 / 0.46 | 7.1e-14 / 0.43 |
| Sclt1 | Ypel1 | 0.0162 / 0.56 | 0.024 / 0.41 | 7.5e-15 / 0.33 |
| Ift172 | Ypel1 | 0.0206 / 0.52 | 0.0059 / 0.5 | 3.9e-24 / 0.31 |
| Upf3a | Ypel1 | 0.0206 / 0.52 | 0.0063 / 0.49 | 1.3e-14 / 0.33 |
| Ribc1 | Ypel1 | 0.0162 / 0.56 | 0.0066 / 0.49 | 8.5e-16 / 0.25 |
| Ttc21b | Tctex1d2 | 0.0260 / 0.49 | 0.046 / 0.36 | 6.8e-18 / 0.27 |
| Xkr8 | Tctex1d2 | 0.0206 / 0.52 | 0.015 / 0.44 | 1.3e-16 / 0.26 |
| Aptx | Tctex1d2 | 0.0177 / 0.54 | 0.029 / 0.39 | 8.8e-16 / 0.25 |
| Tesk1 | Tctex1d2 | 0.0206 / 0.52 | 0.017 / 0.43 | 5e-28 / 0.34 |
| Ift172 | Tctex1d2 | 0.0260 / 0.49 | 0.049 / 0.35 | 1.3e-23 / 0.31 |
| Upf3a | Tctex1d2 | 0.0260 / 0.49 | 0.035 / 0.38 | 1.3e-14 / 0.33 |
| Ssr4 | Tctex1d2 | 0.0237 / 0.50 | 0.035 / 0.38 | 1.7e-29 / 0.29 |
| Btbd3 | Fstl1 | 0.0097 / 0.77 | 0.0042 / 0.52 | 6.1e-22 / 0.41 |
| Ddx20 | Lca5l | 0.0206 / 0.52 | 0.023 / 0.41 | 1.4e-22 / 0.25 |
| Etfb | Sod2 | 0.0134 / 0.59 | 0.0097 / 0.46 | 1.2e-31 / 0.36 |
| Aptx | Tbp | 0.0177 / 0.54 | 0.037 / 0.38 | 1.1e-19 / 0.28 |
| Ulk4 | Tbp | 0.0260 / 0.49 | 0.0016 / 0.62 | 3e-15 / 0.33 |
| Zdhhc4 | Mapk14 | 0.0349 / 0.47 | 0.021 / 0.42 | 1.3e-14 / 0.33 |
| Ulk4 | Efhb | 0.0260 / 0.49 | 0.0089 / 0.47 | 2.6e-14 / 0.27 |
| Upf3a | Cabyr | 0.0260 / 0.49 | 0.004 / 0.53 | 7.2e-14 / 0.27 |
| Svip | Camk4 | 0.0325 / 0.47 | 0.023 / 0.41 | 3.1e-23 / 0.35 |
| Odf2 | Spata24 | 0.0206 / 0.52 | 0.019 / 0.42 | 7.6e-17 / 0.3 |
| Btbd3 | Ppic | 0.0190 / 0.53 | 0.014 / 0.44 | 2.4e-19 / 0.28 |
| Upf3a | Ccdc87 | 0.0206 / 0.52 | 0.02 / 0.42 | 7.2e-14 / 0.27 |
| Upf3a | Spata17 | 0.0177 / 0.54 | 0.02 / 0.42 | 7.2e-14 / 0.27 |
| Xkr8 | Efhc1 | 0.0206 / 0.52 | 0.016 / 0.43 | 2.8e-10 / 0.27 |
| Sclt1 | Stk36 | 0.0206 / 0.52 | 0.012 / 0.45 | 1.1e-15 / 0.34 |
| Aptx | Stk36 | 0.0177 / 0.54 | 0.015 / 0.44 | 5e-18 / 0.27 |
| Polb | Stk36 | 0.0260 / 0.49 | 0.0073 / 0.48 | 9.8e-23 / 0.26 |
| Ankrd49 | Mybl1 | 0.0162 / 0.56 | 0.034 / 0.38 | 1.4e-12 / 0.41 |
| Upf3a | Ppp1r42 | 0.0260 / 0.49 | 0.0088 / 0.47 | 7.2e-14 / 0.27 |
| Odf2 | Nphp1 | 0.0162 / 0.56 | 0.009 / 0.47 | 1.1e-12 / 0.41 |
| Xkr8 | Nphp1 | 0.0162 / 0.56 | 0.017 / 0.43 | 4.2e-11 / 0.28 |
| Txnl4b | Nphp1 | 0.0206 / 0.52 | 0.045 / 0.36 | 3.3e-10 / 0.27 |
| Upf3a | Nphp1 | 0.0206 / 0.52 | 0.034 / 0.38 | 7.5e-11 / 0.38 |
| Col4a1 | Btbd3 | 0.0154 / 0.56 | 0.0015 / 0.63 | 1.4e-21 / 0.4 |
| Col4a2 | Btbd3 | 0.0154 / 0.56 | 0.0022 / 0.58 | 3.3e-21 / 0.4 |
| Odf2 | Kif3b | 0.0206 / 0.52 | 0.017 / 0.43 | 7.6e-17 / 0.3 |
| Sclt1 | Kif3b | 0.0206 / 0.52 | 0.046 / 0.36 | 2.2e-16 / 0.29 |
| Upf3a | Kif3b | 0.0260 / 0.49 | 0.019 / 0.42 | 7.2e-14 / 0.27 |
| Amn1 | Wfdc3 | 0.0260 / 0.49 | 0.012 / 0.45 | 9.4e-17 / 0.26 |
| Ulk4 | Wfdc3 | 0.0260 / 0.49 | 0.015 / 0.43 | 6.4e-15 / 0.33 |
| Ribc1 | Wfdc3 | 0.0206 / 0.52 | 0.015 / 0.44 | 2.9e-18 / 0.27 |
| Gpr160 | Tprn | 0.0362 / 0.46 | 0.0049 / 0.51 | 4.1e-09 / 0.34 |
| Xkr8 | Odf2 | 0.0162 / 0.56 | 0.017 / 0.43 | 2.1e-16 / 0.35 |
| Amn1 | Odf2 | 0.0206 / 0.52 | 0.0026 / 0.56 | 5.8e-17 / 0.35 |
| Wdr62 | Odf2 | 0.0206 / 0.52 | 0.0061 / 0.49 | 1.1e-16 / 0.29 |
| Ulk4 | Odf2 | 0.0206 / 0.52 | 0.0015 / 0.63 | 2.3e-17 / 0.49 |
| Fgfr1 | Fam171a1 | 0.0167 / 0.55 | 0.038 / 0.37 | 2.5e-26 / 0.45 |
| Gdi1 | Pomt1 | 0.0260 / 0.49 | 0.047 / 0.36 | 1.9e-12 / 0.25 |
| Tbx18 | Casq2 | 0.0380 / 0.46 | 0.045 / 0.36 | 2.3e-17 / 0.27 |
| Xkr8 | Ddx20 | 0.0162 / 0.56 | 0.0066 / 0.49 | 4.4e-18 / 0.27 |
| Iqce | Ddx20 | 0.0206 / 0.52 | 0.026 / 0.4 | 1.8e-16 / 0.26 |
| Rnf32 | Ddx20 | 0.0206 / 0.52 | 0.015 / 0.44 | 5.2e-10 / 0.27 |
| Upf3a | Ddx20 | 0.0206 / 0.52 | 0.026 / 0.4 | 1.3e-14 / 0.33 |
| Ribc1 | Ddx20 | 0.0162 / 0.56 | 0.023 / 0.41 | 7.2e-16 / 0.25 |
| Fancd2 | Sass6 | 0.0244 / 0.50 | 0.0012 / 0.65 | 4.1e-17 / 0.26 |
| Upf3a | Lrriq3 | 0.0260 / 0.49 | 0.004 / 0.53 | 1.3e-14 / 0.33 |

| | | | | |
|---|---|---|---|---|
| Xkr8 | Sclt1 | 0.0162 / 0.56 | 0.0073 / 0.48 | 4e-15 / 0.33 |
| Tesk1 | Sclt1 | 0.0162 / 0.56 | 0.016 / 0.43 | 8.3e-17 / 0.35 |
| Styxl1 | Sclt1 | 0.0349 / 0.47 | 0.0055 / 0.5 | 5.1e-15 / 0.33 |
| Rnf32 | Sclt1 | 0.0206 / 0.52 | 0.0055 / 0.5 | 7.5e-11 / 0.38 |
| Lrrc56 | Sclt1 | 0.0206 / 0.52 | 0.012 / 0.45 | 1.3e-14 / 0.27 |
| Wdr62 | Sclt1 | 0.0206 / 0.52 | 0.025 / 0.4 | 3.1e-17 / 0.3 |
| Txnl4b | Sclt1 | 0.0206 / 0.52 | 0.0032 / 0.54 | 1.2e-14 / 0.33 |
| Lrp2bp | Sclt1 | 0.0206 / 0.52 | 0.0032 / 0.54 | 3.6e-15 / 0.33 |
| Lrrc49 | Sclt1 | 0.0206 / 0.52 | 0.0059 / 0.5 | 2e-10 / 0.27 |
| Ribc1 | Sclt1 | 0.0162 / 0.56 | 0.011 / 0.46 | 1.6e-16 / 0.35 |
| Zdhhc4 | Slc50a1 | 0.0349 / 0.47 | 0.021 / 0.42 | 1.3e-14 / 0.33 |
| Tollip | Slc50a1 | 0.0349 / 0.47 | 0.038 / 0.37 | 4.2e-09 / 0.25 |
| Ankrd42 | Xkr8 | 0.0206 / 0.52 | 0.0042 / 0.52 | 1.3e-14 / 0.33 |
| Ulk4 | Xkr8 | 0.0206 / 0.52 | 0.035 / 0.38 | 4.9e-15 / 0.33 |
| Upf3a | Aptx | 0.0177 / 0.54 | 0.02 / 0.42 | 7.5e-12 / 0.29 |
| Lrp2bp | Aptx | 0.0177 / 0.54 | 0.02 / 0.42 | 1.1e-19 / 0.28 |
| Gdi1 | Aptx | 0.0177 / 0.54 | 0.0048 / 0.51 | 3.6e-10 / 0.27 |
| Rnf32 | Tesk1 | 0.0206 / 0.52 | 0.026 / 0.4 | 5.5e-10 / 0.27 |
| Upf3a | Tesk1 | 0.0206 / 0.52 | 0.045 / 0.36 | 1.3e-14 / 0.33 |
| Gdi1 | Tesk1 | 0.0206 / 0.52 | 0.0015 / 0.63 | 5.4e-13 / 0.31 |
| Fancd2 | Cdc7 | 0.0168 / 0.55 | 0.014 / 0.44 | 1.4e-14 / 0.33 |
| Ulk4 | Tchp | 0.0206 / 0.52 | 0.0032 / 0.54 | 1.7e-12 / 0.3 |
| Upf3a | Iqce | 0.0260 / 0.49 | 0.035 / 0.38 | 1.3e-14 / 0.33 |
| Ift172 | Rnf32 | 0.0260 / 0.49 | 0.02 / 0.42 | 2.6e-12 / 0.3 |
| Upf3a | Rnf32 | 0.0260 / 0.49 | 0.004 / 0.53 | 7.5e-11 / 0.38 |
| Arih2 | Rnf32 | 0.0260 / 0.49 | 0.021 / 0.41 | 5.1e-10 / 0.27 |
| Txnl4b | Agbl5 | 0.0206 / 0.52 | 0.0033 / 0.54 | 2.9e-16 / 0.26 |
| Amn1 | Ift172 | 0.0260 / 0.49 | 0.0032 / 0.54 | 7.5e-21 / 0.29 |
| Ulk4 | Ift172 | 0.0260 / 0.49 | 0.005 / 0.51 | 3e-15 / 0.33 |
| Txnl4b | Amn1 | 0.0260 / 0.49 | 0.029 / 0.39 | 1.6e-16 / 0.26 |
| Upf3a | Amn1 | 0.0260 / 0.49 | 0.0055 / 0.5 | 1.3e-14 / 0.33 |
| Arih2 | Amn1 | 0.0260 / 0.49 | 0.0048 / 0.51 | 1.6e-16 / 0.26 |
| C2cd3 | Kdm3a | 0.0239 / 0.50 | 0.021 / 0.41 | 2.6e-08 / 0.32 |
| Amotl2 | Lig1 | 0.0369 / 0.46 | 0.044 / 0.36 | 9.7e-16 / 0.34 |
| Upf3a | Wdr93 | 0.0260 / 0.49 | 0.0029 / 0.55 | 7.5e-12 / 0.29 |
| Ribc1 | Ankrd42 | 0.0206 / 0.52 | 0.0059 / 0.5 | 1.3e-14 / 0.33 |
| Upf3a | Txnl4b | 0.0260 / 0.49 | 0.0022 / 0.58 | 1.3e-14 / 0.33 |
| Lrp2bp | Upf3a | 0.0260 / 0.49 | 0.02 / 0.42 | 1.3e-14 / 0.33 |
| Ulk4 | Upf3a | 0.0260 / 0.49 | 0.0032 / 0.54 | 1.5e-15 / 0.46 |
| Fam118b | Upf3a | 0.0260 / 0.49 | 0.004 / 0.53 | 1.3e-14 / 0.33 |
| Spa17 | Upf3a | 0.0260 / 0.49 | 0.035 / 0.38 | 1.3e-14 / 0.33 |
| Ulk4 | Polb | 0.0260 / 0.49 | 0.032 / 0.39 | 1.7e-19 / 0.32 |
| Fam118b | Lrp2bp | 0.0260 / 0.49 | 0.011 / 0.46 | 6.2e-20 / 0.28 |
| Ribc1 | Fam118b | 0.0206 / 0.52 | 0.0048 / 0.51 | 3.7e-18 / 0.27 |

Table S3: A total of 85 reproducible second-order rewired gene pairs between human and mouse ectoderm derived tissue types. Gene pairs with their second-order differential $P$-values and effect sizes $\varepsilon$ are shown as obtained from FANTOM5, Yang et al. and Evo-devo datasets, respectively.

| **Gene** | **Gene** | **FANTOM5** | **Yang el al.** | **Evo-devo** |
|---|---|---|---|---|
| | | $P$-value / Effect size $\varepsilon$ | $P$-value / Effect size $\varepsilon$ | $P$-value / Effect size $\varepsilon$ |
| PKP3 | TMEM200A | 0.042 / 0.57 | 0.018 / 0.52 | 8.3e-11 / 0.35 |
| PKP3 | UNC5B | 0.042 / 0.57 | 0.0085 / 0.59 | 1.4e-10 / 0.35 |
| UST | TSPAN15 | 0.027 / 0.73 | 0.0054 / 0.63 | 0.00034 / 0.27 |
| TACC1 | UST | 0.047 / 0.55 | 0.015 / 0.54 | 0.00047 / 0.26 |
| NRIP2 | SASH1 | 0.042 / 0.56 | 0.036 / 0.46 | 1.2e-08 / 0.31 |
| ST6GALNAC5 | PGAM2 | 0.027 / 0.75 | 0.0016 / 0.77 | 2.5e-11 / 0.49 |
| HSPA12A | XRCC3 | 0.027 / 0.80 | 0.012 / 0.56 | 6.1e-09 / 0.32 |
| EPHB2 | INF2 | 0.027 / 0.68 | 0.0076 / 0.6 | 2.4e-07 / 0.38 |
| ETS2 | TIAM1 | 0.040 / 0.58 | 0.0045 / 0.65 | 2e-15 / 0.58 |
| SEL1L3 | ETS2 | 0.027 / 0.79 | 0.017 / 0.53 | 7.5e-16 / 0.59 |
| FZD7 | SH3BGR | 0.034 / 0.61 | 0.0058 / 0.63 | 1.4e-14 / 0.41 |
| SHF | SH3BGR | 0.042 / 0.56 | 0.0022 / 0.73 | 2.7e-14 / 0.56 |
| FOXP1 | SH3BGR | 0.027 / 0.75 | 0.011 / 0.56 | 1.4e-17 / 0.46 |
| SNRK | SH3BGR | 0.027 / 0.68 | 0.028 / 0.49 | 5.5e-14 / 0.55 |
| ADRB1 | TNFSF9 | 0.034 / 0.60 | 0.0029 / 0.69 | 1.1e-10 / 0.47 |
| CCDC88B | ALDH1A1 | 0.027 / 0.75 | 0.0034 / 0.68 | 8.7e-10 / 0.33 |
| PTPN9 | TOMM40L | 0.042 / 0.57 | 0.012 / 0.56 | 5.7e-09 / 0.43 |
| SLC31A2 | CAPN3 | 0.028 / 0.67 | 0.01 / 0.57 | 1.2e-11 / 0.37 |
| SH3BGRL | F3 | 0.042 / 0.57 | 0.019 / 0.51 | 9.8e-12 / 0.5 |
| TMSB10 | ZMAT3 | 0.034 / 0.60 | 0.019 / 0.52 | 5.5e-10 / 0.45 |
| CCDC120 | TNC | 0.044 / 0.56 | 0.033 / 0.47 | 0.00035 / 0.27 |
| SMPD3 | KNDC1 | 0.028 / 0.66 | 0.016 / 0.53 | 6.4e-08 / 0.3 |
| MYBBP1A | NACA | 0.034 / 0.61 | 0.0064 / 0.61 | 1.4e-05 / 0.32 |
| ANKRD46 | NCOA7 | 0.034 / 0.61 | 0.041 / 0.45 | 9.2e-09 / 0.42 |
| SBK1 | CNKSR3 | 0.048 / 0.54 | 0.0011 / 0.82 | 2.7e-06 / 0.26 |
| ACYP1 | PREP | 0.028 / 0.64 | 0.0086 / 0.59 | 0.00017 / 0.28 |
| NTN4 | PKIB | 0.028 / 0.66 | 0.0016 / 0.76 | 2.1e-11 / 0.36 |
| SMARCAL1 | SPOCK2 | 0.049 / 0.54 | 0.026 / 0.49 | 1.5e-08 / 0.42 |
| SLC7A6 | SGPL1 | 0.027 / 0.73 | 0.037 / 0.46 | 3e-04 / 0.27 |
| EML1 | PCBP3 | 0.040 / 0.57 | 0.0024 / 0.71 | 3.6e-09 / 0.43 |
| AQP7 | PCBP3 | 0.040 / 0.57 | 0.018 / 0.52 | 2.2e-07 / 0.29 |
| BMP1 | NTN4 | 0.027 / 0.69 | 0.019 / 0.52 | 2.2e-09 / 0.44 |
| CERK | TTYH2 | 0.027 / 0.68 | 0.0011 / 0.82 | 3.6e-08 / 0.4 |
| SGPP2 | TTYH2 | 0.027 / 0.70 | 0.023 / 0.5 | 1.3e-07 / 0.29 |
| GNAL | UBE2O | 0.043 / 0.56 | 0.012 / 0.56 | 5.4e-06 / 0.34 |
| LRRC10B | RAB40B | 0.047 / 0.55 | 0.045 / 0.44 | 4.4e-07 / 0.28 |
| FGF7 | STK10 | 0.028 / 0.64 | 0.004 / 0.66 | 1.2e-11 / 0.5 |
| PTPN18 | TRIM7 | 0.049 / 0.54 | 0.044 / 0.44 | 1.4e-08 / 0.42 |
| ARHGEF37 | SLC22A4 | 0.042 / 0.57 | 0.01 / 0.57 | 2.3e-11 / 0.36 |
| PCDHB12 | TRPV2 | 0.040 / 0.57 | 0.016 / 0.53 | 1.4e-08 / 0.26 |
| ENPP2 | KCNAB3 | 0.041 / 0.57 | 0.0095 / 0.58 | 1.5e-08 / 0.41 |
| HSPB8 | RNF43 | 0.028 / 0.66 | 0.0064 / 0.61 | 8.8e-11 / 0.35 |
| TMEM106B | TMEM100 | 0.043 / 0.56 | 0.009 / 0.58 | 2.1e-10 / 0.46 |
| DHDDS | EML1 | 0.032 / 0.63 | 0.0016 / 0.76 | 1.9e-11 / 0.49 |
| TRIM9 | PTPRN2 | 0.034 / 0.61 | 0.01 / 0.57 | 9.4e-11 / 0.35 |
| SFXN4 | RRM2 | 0.032 / 0.62 | 0.012 / 0.56 | 2.8e-11 / 0.36 |
| POLE | F13A1 | 0.032 / 0.62 | 0.017 / 0.53 | 4.1e-17 / 0.45 |
| FGF7 | SLC9A3 | 0.028 / 0.64 | 0.00098 / 0.85 | 2.9e-13 / 0.39 |
| MAP4K1 | PCSK1 | 0.028 / 0.64 | 0.045 / 0.44 | 5.5e-08 / 0.4 |
| PPTC7 | ITIH3 | 0.042 / 0.56 | 0.0024 / 0.71 | 4.8e-07 / 0.28 |
| LPCAT4 | ENPP2 | 0.028 / 0.64 | 0.039 / 0.45 | 0.00029 / 0.27 |
| LCAT | ENPP2 | 0.028 / 0.64 | 0.0038 / 0.66 | 1.1e-08 / 0.42 |
| GPN1 | LRRC24 | 0.040 / 0.57 | 0.0031 / 0.69 | 1.6e-08 / 0.31 |
| SDR42E1 | SLC7A4 | 0.034 / 0.59 | 0.037 / 0.46 | 2.6e-16 / 0.27 |
| FBXO2 | PIGP | 0.040 / 0.57 | 0.034 / 0.47 | 5.2e-16 / 0.43 |
| DHDDS | MRPS34 | 0.034 / 0.61 | 0.04 / 0.45 | 1.3e-05 / 0.32 |
| GNAI3 | RPUSD1 | 0.034 / 0.59 | 0.043 / 0.44 | 6.8e-09 / 0.42 |
| ALS2 | ADAMTS10 | 0.028 / 0.64 | 0.0063 / 0.62 | 3.9e-11 / 0.36 |
| TRO | NRXN1 | 0.028 / 0.65 | 0.034 / 0.47 | 8.1e-08 / 0.29 |
| ABCG4 | PCDHB12 | 0.034 / 0.59 | 0.043 / 0.45 | 4.3e-18 / 0.64 |
| ADAP1 | GNAL | 0.027 / 0.67 | 0.043 / 0.44 | 6.9e-05 / 0.29 |

| | | | | |
|---|---|---|---|---|
| CKS1B | PHLPP1 | 0.027 / 0.67 | 0.03 / 0.48 | 6.5e-10 / 0.45 |
| ARRDC4 | KCNJ10 | 0.027 / 0.67 | 0.037 / 0.46 | 1.8e-08 / 0.41 |
| DISP2 | BPNT1 | 0.032 / 0.62 | 0.03 / 0.48 | 5e-14 / 0.4 |
| DHDDS | PLEKHM3 | 0.032 / 0.63 | 0.012 / 0.56 | 1.6e-12 / 0.52 |
| CSRNP3 | DNER | 0.034 / 0.62 | 0.03 / 0.48 | 0.00027 / 0.27 |
| RHOF | NGEF | 0.047 / 0.55 | 0.025 / 0.5 | 3e-07 / 0.28 |
| ARRDC4 | RCN1 | 0.035 / 0.59 | 0.0033 / 0.68 | 1.3e-13 / 0.54 |
| SS18L1 | SLC12A6 | 0.043 / 0.56 | 0.0081 / 0.59 | 1.5e-14 / 0.41 |
| PXN | FGF7 | 0.034 / 0.59 | 0.016 / 0.53 | 3.7e-14 / 0.55 |
| TLL1 | FGF7 | 0.042 / 0.57 | 0.0022 / 0.73 | 0.00019 / 0.28 |
| PPP1R3F | DTD1 | 0.032 / 0.62 | 0.036 / 0.46 | 6.8e-15 / 0.42 |
| TBCEL | SS18L1 | 0.040 / 0.58 | 0.037 / 0.46 | 4.3e-07 / 0.37 |
| GPRC5B | ARHGAP15 | 0.027 / 0.67 | 0.013 / 0.55 | 1.3e-09 / 0.33 |
| DLAT | BCL9 | 0.027 / 0.67 | 0.018 / 0.52 | 1.4e-05 / 0.32 |
| MAST3 | RAVER2 | 0.039 / 0.58 | 0.0085 / 0.59 | 2.9e-11 / 0.49 |
| AQP7 | DHDDS | 0.032 / 0.63 | 0.011 / 0.56 | 1.3e-08 / 0.31 |
| HS3ST1 | GALNT12 | 0.032 / 0.62 | 0.006 / 0.62 | 2.6e-14 / 0.34 |
| MAP4K1 | SLC24A2 | 0.028 / 0.64 | 0.0069 / 0.61 | 1.6e-11 / 0.49 |
| TMEM123 | LRRC8B | 0.027 / 0.78 | 0.012 / 0.56 | 1.6e-07 / 0.29 |
| TUBGCP2 | FLT1 | 0.042 / 0.57 | 0.026 / 0.49 | 2.5e-05 / 0.31 |
| TMEM135 | ENO2 | 0.043 / 0.56 | 0.006 / 0.62 | 6.4e-19 / 0.47 |
| NELL1 | SCRN1 | 0.041 / 0.57 | 0.012 / 0.55 | 1.2e-09 / 0.33 |
| ENPP6 | ARRDC4 | 0.029 / 0.64 | 0.01 / 0.57 | 3e-09 / 0.43 |
| ABHD8 | TMCO3 | 0.028 / 0.65 | 0.038 / 0.46 | 1e-20 / 0.37 |

Table S4: A total of 57 reproducible second-order rewired gene pairs between human and mouse primitive streak derived tissue types. Gene pairs with their second-order differential $P$-values and effect sizes $\varepsilon$ are shown as obtained from FANTOM5, Yang et al. and Evo-devo datasets, respectively.

| **Gene** | **Gene** | **FANTOM5** | **Yang el al.** | **Evo-devo** |
|---|---|---|---|---|
| | | $P$-value / Effect size $\varepsilon$ | $P$-value / Effect size $\varepsilon$ | $P$-value / Effect size $\varepsilon$ |
| MBD1 | PFN4 | 0.0147 / 0.50 | 3.2e-05 / 0.39 | 1e-07 / 0.27 |
| PIAS2 | MBD1 | 0.0147 / 0.50 | 0.00013 / 0.47 | 2e-07 / 0.27 |
| AGBL5 | MBD1 | 0.0147 / 0.50 | 0.00013 / 0.47 | 2e-07 / 0.27 |
| ACRBP | MBD1 | 0.0090 / 0.53 | 4.5e-05 / 0.51 | 2.7e-07 / 0.26 |
| FAM71E1 | MBD1 | 0.0147 / 0.50 | 4.5e-05 / 0.51 | 2.7e-07 / 0.26 |
| RABEPK | PSMC3IP | 0.0088 / 0.53 | 0.00057 / 0.43 | 3.4e-19 / 0.28 |
| XKR8 | AMZ2 | 0.0063 / 0.57 | 0.00045 / 0.34 | 8.4e-28 / 0.29 |
| PLK4 | FBXO48 | 0.0063 / 0.57 | 0.0027 / 0.37 | 3.9e-18 / 0.32 |
| TACC3 | FBXO48 | 0.0281 / 0.46 | 0.004 / 0.36 | 1.6e-21 / 0.35 |
| EZH2 | FBXO48 | 0.0281 / 0.46 | 0.0064 / 0.34 | 3.6e-19 / 0.33 |
| TTK | FBXO48 | 0.0147 / 0.50 | 0.0027 / 0.37 | 7.4e-21 / 0.35 |
| RABEPK | CDKL3 | 0.0172 / 0.49 | 0.0051 / 0.35 | 2.9e-24 / 0.52 |
| XKR8 | CDKL3 | 0.0172 / 0.49 | 7.3e-05 / 0.49 | 8.4e-28 / 0.29 |
| SNAP29 | COIL | 0.0063 / 0.57 | 0.0053 / 0.35 | 1.1e-20 / 0.35 |
| RABEPK | COIL | 0.0088 / 0.53 | 0.00056 / 0.43 | 2.9e-24 / 0.52 |
| XKR8 | COIL | 0.0063 / 0.57 | 4.6e-05 / 0.5 | 8.4e-28 / 0.29 |
| SPAG4 | CCNK | 0.0063 / 0.57 | 0.0077 / 0.33 | 1.6e-07 / 0.27 |
| RABEPK | CCNK | 0.0079 / 0.54 | 0.00014 / 0.47 | 2.3e-23 / 0.51 |
| XKR8 | CCNK | 0.0061 / 0.59 | 4e-05 / 0.51 | 8e-22 / 0.26 |
| ZC3H14 | ACTR10 | 0.0061 / 0.61 | 0.0038 / 0.36 | 2.1e-19 / 0.33 |
| TTC21B | HSPA2 | 0.0061 / 0.60 | 0.0016 / 0.39 | 1.3e-14 / 0.29 |
| RABEPK | ACYP1 | 0.0112 / 0.52 | 0.00012 / 0.47 | 4.7e-22 / 0.36 |
| PM20D1 | GSTZ1 | 0.0241 / 0.47 | 0.00071 / 0.42 | 2.7e-21 / 0.29 |
| MEA1 | NOL8 | 0.0080 / 0.54 | 0.0019 / 0.39 | 8.3e-16 / 0.3 |
| XKR8 | TBP | 0.0063 / 0.57 | 0.00093 / 0.41 | 1.7e-23 / 0.27 |
| RABEPK | PPP1R11 | 0.0079 / 0.54 | 0.0028 / 0.37 | 1.4e-20 / 0.25 |
| RABEPK | SPATA24 | 0.0088 / 0.53 | 0.0015 / 0.39 | 2.2e-24 / 0.52 |
| XKR8 | SPATA24 | 0.0063 / 0.57 | 0.00021 / 0.46 | 8.6e-27 / 0.29 |
| APLNR | PDGFRB | 0.0283 / 0.46 | 0.0011 / 0.4 | 1.4e-11 / 0.34 |
| XKR8 | PIAS2 | 0.0063 / 0.57 | 0.00012 / 0.48 | 8.4e-28 / 0.29 |
| POLE | NSL1 | 0.0172 / 0.49 | 0.0012 / 0.4 | 2.7e-10 / 0.32 |
| XKR8 | NPHP1 | 0.0063 / 0.57 | 0.00013 / 0.36 | 1.7e-23 / 0.27 |
| APOOL | MKKS | 0.0274 / 0.46 | 0.0035 / 0.36 | 5.8e-18 / 0.32 |
| RABEPK | SPAG4 | 0.0088 / 0.53 | 0.0011 / 0.4 | 2.2e-24 / 0.52 |
| FAM118B | SPAG4 | 0.0072 / 0.55 | 0.0026 / 0.37 | 1.1e-22 / 0.36 |
| EFHC2 | SPAG4 | 0.0061 / 0.60 | 0.0018 / 0.39 | 5.1e-23 / 0.37 |
| TTC21B | TCEA2 | 0.0060 / 0.63 | 6.8e-05 / 0.49 | 1.4e-29 / 0.3 |
| SCLT1 | TCEA2 | 0.0061 / 0.61 | 0.001 / 0.41 | 1.1e-21 / 0.26 |
| DDX20 | RABEPK | 0.0063 / 0.57 | 0.0015 / 0.39 | 2.9e-24 / 0.52 |
| SCLT1 | RABEPK | 0.0072 / 0.55 | 0.0012 / 0.4 | 2.1e-22 / 0.36 |
| XKR8 | RABEPK | 0.0079 / 0.54 | 0.00061 / 0.42 | 7.1e-22 / 0.26 |
| UBXN11 | RABEPK | 0.0079 / 0.54 | 0.00056 / 0.43 | 1.3e-21 / 0.29 |
| LRRC8B | RABEPK | 0.0072 / 0.55 | 0.0039 / 0.36 | 1.2e-23 / 0.37 |
| AGBL5 | RABEPK | 0.0088 / 0.53 | 0.0028 / 0.37 | 2.9e-24 / 0.52 |
| PHKG2 | RABEPK | 0.0088 / 0.53 | 0.0015 / 0.39 | 1.7e-20 / 0.25 |
| FAM71E1 | RABEPK | 0.0088 / 0.53 | 0.0015 / 0.39 | 1.7e-24 / 0.52 |
| UPF3A | RABEPK | 0.0088 / 0.53 | 0.001 / 0.41 | 7.2e-21 / 0.29 |
| POLB | RABEPK | 0.0079 / 0.54 | 0.00049 / 0.43 | 1.2e-23 / 0.37 |
| FAM118B | RABEPK | 0.0088 / 0.53 | 2.3e-05 / 0.53 | 1.3e-21 / 0.35 |
| RWDD2A | RABEPK | 0.0088 / 0.53 | 0.00027 / 0.45 | 2.8e-10 / 0.32 |
| XKR8 | DDX20 | 0.0172 / 0.49 | 0.00021 / 0.46 | 8.4e-28 / 0.29 |
| ECHS1 | ST3GAL3 | 0.0262 / 0.46 | 8.9e-06 / 0.56 | 3.9e-14 / 0.38 |
| TESK1 | XKR8 | 0.0061 / 0.59 | 0.00075 / 0.42 | 5.9e-26 / 0.28 |
| AGBL5 | XKR8 | 0.0063 / 0.57 | 0.00012 / 0.48 | 8.4e-28 / 0.29 |
| AMN1 | XKR8 | 0.0255 / 0.46 | 0.00018 / 0.36 | 8.4e-28 / 0.29 |
| FAM71E1 | XKR8 | 0.0063 / 0.57 | 0.00021 / 0.46 | 5.9e-26 / 0.28 |
| SPA17 | XKR8 | 0.0061 / 0.59 | 0.00021 / 0.46 | 1.5e-22 / 0.27 |

## G Biological pathways enriched with genes in second-order rewiring during mammalian development

We found pathways that are highly enriched in genes involved in 2nd-order rewired gene interactions in all four species-tissue comparisons. We first obtained the genes involved in significant 2nd-order differential co-expressed patterns in each comparison. Then, we found the common genes among all three datasets: FANTOM5, Evo-devo and Yang el al.. The obtained common genes are then used to perform SIGORA analysis (Foroushani et al., 2013) to identify enriched pathways.

### G.1 Pathways enriched in human ectoderm versus primitive streak derived tissue types

*Comparison 1: Human ectoderm versus primitive streak derived tissue groups.* The significant second-order differential patterns obtained from rewiring pipeline for FANTOM5 et al., Evo-devo and Yang et al. are utilized to find 4,599 common genes. The obtained genes are supplied to a R function SIGORA (Foroushani et al., 2013) which statistically links genes to pathways using a KEGG repository which contains information about all the pathways and involved genes. Using the human KEGG repository (Kanehisa and Goto, 2000) and common genes, returned 56 enriched pathways post Bonferroni correction (Dunnett, 1955) ($P \leq 0.05$). Table S5, shows all 56 enriched pathways with Kegg pathway id, description, the Bonferroni adjusted p-value, number of successes and the pathway size.

Table S5: Biological pathways enriched with rewired second-order gene-gene differential patterns between human ectoderm and primitive streak.

| KEGG Pathway ID | Description | Bonferroni | Successes | Pathway Size |
|---|---|---|---|---|
| hsa04360 | Axon guidance | 0.0e+00 | 99 | 181.00 |
| hsa04010 | MAPK signaling pathway | 8.0e-263 | 123 | 294.00 |
| hsa04110 | Cell cycle | 8.1e-183 | 58 | 124.00 |
| hsa04530 | Tight junction | 4.3e-145 | 73 | 169.00 |
| hsa04015 | Rap1 signaling pathway | 1.1e-97 | 91 | 210.00 |
| hsa04310 | Wnt signaling pathway | 3.0e-93 | 66 | 160.00 |
| hsa04261 | Adrenergic signaling in cardiomyocytes | 1.4e-85 | 66 | 150.00 |
| hsa04510 | Focal adhesion | 2.8e-83 | 92 | 201.00 |
| hsa04910 | Insulin signaling pathway | 6.0e-82 | 58 | 137.00 |
| hsa04390 | Hippo signaling pathway | 2.6e-79 | 71 | 157.00 |
| hsa04210 | Apoptosis | 1.2e-69 | 56 | 136.00 |
| hsa04144 | Endocytosis | 7.4e-67 | 79 | 252.00 |
| hsa05202 | Transcriptional misregulation in cancer | 9.2e-65 | 61 | 192.00 |
| hsa04810 | Regulation of actin cytoskeleton | 3.3e-64 | 90 | 218.00 |
| hsa05412 | Arrhythmogenic right ventricular cardiomyopathy (ARVC) | 4.8e-59 | 41 | 77.00 |
| hsa03030 | DNA replication | 1.4e-57 | 23 | 36.00 |
| hsa04142 | Lysosome | 6.4e-57 | 46 | 128.00 |
| hsa04014 | Ras signaling pathway | 1.3e-54 | 85 | 232.00 |
| hsa04931 | Insulin resistance | 3.6e-54 | 53 | 108.00 |
| hsa04340 | Hedgehog signaling pathway | 4.8e-47 | 25 | 50.00 |
| hsa05205 | Proteoglycans in cancer | 2.3e-36 | 80 | 205.00 |
| hsa04911 | Insulin secretion | 3.8e-36 | 38 | 86.00 |
| hsa04350 | TGF-beta signaling pathway | 4.6e-33 | 35 | 94.00 |
| hsa04068 | FoxO signaling pathway | 1.7e-30 | 50 | 131.00 |
| hsa05166 | HTLV-I infection | 4.0e-28 | 77 | 219.00 |
| hsa00564 | Glycerophospholipid metabolism | 2.1e-23 | 35 | 98.00 |
| hsa04218 | Cellular senescence | 2.1e-22 | 59 | 156.00 |
| hsa00100 | Steroid biosynthesis | 5.5e-22 | 11 | 20.00 |
| hsa00860 | Porphyrin and chlorophyll metabolism | 9.1e-21 | 15 | 42.00 |
| hsa05120 | Epithelial cell signaling in Helicobacter pylori infection | 1.7e-20 | 31 | 70.00 |
| hsa04921 | Oxytocin signaling pathway | 1.4e-18 | 56 | 154.00 |
| hsa05231 | Choline metabolism in cancer | 3.7e-18 | 41 | 98.00 |
| hsa04071 | Sphingolipid signaling pathway | 7.9e-18 | 49 | 119.00 |
| hsa00900 | Terpenoid backbone biosynthesis | 6.1e-17 | 13 | 22.00 |
| hsa00280 | Valine, leucine and isoleucine degradation | 6.7e-17 | 22 | 48.00 |
| hsa04710 | Circadian rhythm | 1.6e-16 | 16 | 31.00 |
| hsa04670 | Leukocyte transendothelial migration | 8.0e-16 | 46 | 114.00 |
| hsa04514 | Cell adhesion molecules (CAMs) | 2.2e-14 | 44 | 149.00 |
| hsa01200 | Carbon metabolism | 2.4e-14 | 49 | 0.00 |
| hsa04151 | PI3K-Akt signaling pathway | 6.6e-14 | 123 | 354.00 |

| | | | | |
|---|---|---|---|---|
| hsa04070 | Phosphatidylinositol signaling system | 8.0e-14 | 38 | 97.00 |
| hsa05132 | Salmonella infection | 1.1e-13 | 30 | 249.00 |
| hsa03460 | Fanconi anemia pathway | 2.0e-13 | 20 | 54.00 |
| hsa05221 | Acute myeloid leukemia | 3.1e-13 | 31 | 67.00 |
| hsa05222 | Small cell lung cancer | 1.8e-12 | 42 | 92.00 |
| hsa04072 | Phospholipase D signaling pathway | 4.8e-12 | 55 | 148.00 |
| hsa04914 | Progesterone-mediated oocyte maturation | 8.3e-12 | 39 | 100.00 |
| hsa04152 | AMPK signaling pathway | 1.3e-11 | 48 | 120.00 |
| hsa04520 | Adherens junction | 1.4e-11 | 33 | 71.00 |
| hsa04024 | cAMP signaling pathway | 1.7e-11 | 78 | 216.00 |
| hsa00562 | Inositol phosphate metabolism | 2.8e-11 | 30 | 73.00 |
| hsa04666 | Fc gamma R-mediated phagocytosis | 3.5e-11 | 35 | 97.00 |
| hsa00270 | Cysteine and methionine metabolism | 5.0e-11 | 19 | 50.00 |
| hsa04512 | ECM-receptor interaction | 5.7e-11 | 36 | 88.00 |
| hsa00604 | Glycosphingolipid biosynthesis - ganglio series | 3.5e-10 | 8 | 15.00 |
| hsa05220 | Chronic myeloid leukemia | 4.6e-10 | 32 | 76.00 |

## G.2 Pathways enriched in mouse ectoderm versus primitive streak derived groups

*Comparison 2: Mouse ectoderm versus primitive streak derived tissue groups.* The significant second-order differential patterns obtained from rewiring pipeline for FANTOM5 et al., Evo-devo and Yang et al. are utilized to find 7,345 common genes for this comparison. We supplied common genes and using mouse KEGG repository (Kanehisa and Goto, 2000) we obtained 89 enriched pathways post Bonferroni correction (Dunnett, 1955) ($P \leq 0.05$). Table S6, shows all 89 enriched pathways with Kegg pathway id, description, the Bonferroni adjusted p-value, number of successes and the pathway size.

Table S6: Biological pathways enriched with rewired second-order gene-gene differential patterns between mouse ectoderm and primitive streak.

| KEGG Pathway ID | Description | Bonferroni | Successes | Pathway Size |
|---|---|---|---|---|
| mmu04010 | MAPK signaling pathway | 0.0e+00 | 175 | 294.00 |
| mmu04360 | Axon guidance | 0.0e+00 | 133 | 180.00 |
| mmu04110 | Cell cycle | 2.3e-302 | 88 | 123.00 |
| mmu04144 | Endocytosis | 2.1e-166 | 134 | 273.00 |
| mmu04142 | Lysosome | 1.9e-148 | 77 | 131.00 |
| mmu04530 | Tight junction | 1.0e-142 | 98 | 167.00 |
| mmu04146 | Peroxisome | 9.4e-117 | 54 | 86.00 |
| mmu04015 | Rap1 signaling pathway | 5.2e-114 | 134 | 214.00 |
| mmu04014 | Ras signaling pathway | 3.9e-109 | 128 | 232.00 |
| mmu05205 | Proteoglycans in cancer | 4.1e-98 | 128 | 205.00 |
| mmu04115 | p53 signaling pathway | 1.4e-91 | 53 | 72.00 |
| mmu04141 | Protein processing in endoplasmic reticulum | 3.4e-82 | 88 | 172.00 |
| mmu04931 | Insulin resistance | 2.2e-72 | 77 | 110.00 |
| mmu05202 | Transcriptional misregulation in cancer | 1.3e-71 | 96 | 223.00 |
| mmu04390 | Hippo signaling pathway | 4.8e-71 | 99 | 157.00 |
| mmu04510 | Focal adhesion | 3.7e-62 | 129 | 201.00 |
| mmu04210 | Apoptosis | 1.3e-61 | 86 | 136.00 |
| mmu04068 | FoxO signaling pathway | 1.0e-60 | 82 | 131.00 |
| mmu04810 | Regulation of actin cytoskeleton | 2.4e-58 | 124 | 220.00 |
| mmu00562 | Inositol phosphate metabolism | 2.0e-55 | 55 | 72.00 |
| mmu00564 | Glycerophospholipid metabolism | 5.9e-51 | 56 | 98.00 |
| mmu04151 | PI3K-Akt signaling pathway | 8.0e-50 | 196 | 359.00 |
| mmu04330 | Notch signaling pathway | 1.4e-48 | 37 | 54.00 |
| mmu03030 | DNA replication | 1.1e-47 | 28 | 35.00 |
| mmu04350 | TGF-beta signaling pathway | 6.6e-46 | 55 | 95.00 |
| mmu04070 | Phosphatidylinositol signaling system | 2.4e-45 | 67 | 96.00 |
| mmu04261 | Adrenergic signaling in cardiomyocytes | 1.3e-44 | 88 | 152.00 |
| mmu05412 | Arrhythmogenic right ventricular cardiomyopathy (ARVC) | 4.6e-43 | 50 | 77.00 |

| | | | | |
|---|---|---|---|---|
| mmu04150 | mTOR signaling pathway | 8.0e-42 | 86 | 156.00 |
| mmu04512 | ECM-receptor interaction | 7.0e-41 | 57 | 88.00 |
| mmu04340 | Hedgehog signaling pathway | 5.3e-38 | 33 | 52.00 |
| mmu04910 | Insulin signaling pathway | 9.4e-37 | 76 | 139.00 |
| mmu04520 | Adherens junction | 1.3e-36 | 47 | 71.00 |
| mmu04216 | Ferroptosis | 9.2e-34 | 29 | 40.00 |
| mmu04120 | Ubiquitin mediated proteolysis | 9.8e-33 | 71 | 146.00 |
| mmu04722 | Neurotrophin signaling pathway | 1.3e-32 | 71 | 121.00 |
| mmu00532 | Glycosaminoglycan biosynthesis - chondroitin sulfate / dermatan sulfate | 1.3e-30 | 16 | 20.00 |
| mmu05231 | Choline metabolism in cancer | 8.2e-30 | 60 | 98.00 |
| mmu04137 | Mitophagy - animal | 1.9e-29 | 41 | 66.00 |
| mmu04072 | Phospholipase D signaling pathway | 5.6e-29 | 87 | 149.00 |
| mmu04710 | Circadian rhythm | 2.2e-28 | 23 | 30.00 |
| mmu05166 | HTLV-I infection | 1.0e-26 | 121 | 248.00 |
| mmu04310 | Wnt signaling pathway | 1.1e-26 | 91 | 162.00 |
| mmu01200 | Carbon metabolism | 1.8e-23 | 72 | 0.00 |
| mmu04211 | Longevity regulating pathway | 2.1e-22 | 58 | 90.00 |
| mmu04914 | Progesterone-mediated oocyte maturation | 3.0e-22 | 58 | 90.00 |
| mmu04218 | Cellular senescence | 6.2e-21 | 97 | 185.00 |
| mmu01521 | EGFR tyrosine kinase inhibitor resistance | 6.9e-21 | 51 | 0.00 |
| mmu04071 | Sphingolipid signaling pathway | 2.9e-19 | 76 | 124.00 |
| mmu04136 | Autophagy - other | 8.9e-19 | 20 | 32.00 |
| mmu05132 | Salmonella infection | 3.2e-18 | 43 | 253.00 |
| mmu04933 | AGE-RAGE signaling pathway in diabetic complications | 1.0e-16 | 70 | 101.00 |
| mmu04152 | AMPK signaling pathway | 2.8e-15 | 77 | 126.00 |
| mmu05224 | Breast cancer | 1.2e-14 | 85 | 147.00 |
| mmu04140 | Autophagy - animal | 1.4e-14 | 78 | 138.00 |
| mmu04911 | Insulin secretion | 4.4e-14 | 53 | 86.00 |
| mmu00520 | Amino sugar and nucleotide sugar metabolism | 2.6e-13 | 29 | 50.00 |
| mmu04932 | Non-alcoholic fatty liver disease (NAFLD) | 5.4e-13 | 86 | 151.00 |
| mmu04666 | Fc gamma R-mediated phagocytosis | 8.2e-13 | 53 | 92.00 |
| mmu00534 | Glycosaminoglycan biosynthesis - heparan sulfate / heparin | 8.6e-13 | 16 | 24.00 |
| mmu00640 | Propanoate metabolism | 5.2e-12 | 26 | 34.00 |
| mmu00604 | Glycosphingolipid biosynthesis - ganglio series | 5.7e-12 | 12 | 15.00 |
| mmu04611 | Platelet activation | 2.8e-11 | 76 | 124.00 |
| mmu00280 | Valine, leucine and isoleucine degradation | 4.4e-11 | 33 | 57.00 |
| mmu04114 | Oocyte meiosis | 2.4e-10 | 70 | 119.00 |
| mmu01522 | Endocrine resistance | 2.2e-09 | 60 | 0.00 |
| mmu00514 | Other types of O-glycan biosynthesis | 6.8e-09 | 15 | 43.00 |
| mmu05222 | Small cell lung cancer | 7.5e-09 | 65 | 93.00 |
| mmu05014 | Amyotrophic lateral sclerosis (ALS) | 1.4e-08 | 31 | 370.00 |
| mmu04540 | Gap junction | 2.2e-08 | 51 | 86.00 |
| mmu00510 | N-Glycan biosynthesis | 8.4e-08 | 30 | 50.00 |
| mmu05220 | Chronic myeloid leukemia | 8.7e-08 | 46 | 76.00 |
| mmu00130 | Ubiquinone and other terpenoid-quinone biosynthesis | 2.1e-07 | 8 | 11.00 |
| mmu04713 | Circadian entrainment | 5.3e-07 | 51 | 98.00 |
| mmu00020 | Citrate cycle (TCA cycle) | 7.4e-07 | 24 | 32.00 |
| mmu04923 | Regulation of lipolysis in adipocytes | 9.1e-07 | 37 | 56.00 |
| mmu00260 | Glycine, serine and threonine metabolism | 9.4e-07 | 24 | 40.00 |
| mmu05152 | Tuberculosis | 1.1e-06 | 79 | 180.00 |
| mmu04657 | IL-17 signaling pathway | 2.4e-06 | 42 | 91.00 |
| mmu01212 | Fatty acid metabolism | 2.9e-06 | 36 | 0.00 |
| mmu03410 | Base excision repair | 3.5e-06 | 22 | 34.00 |
| mmu03440 | Homologous recombination | 4.3e-06 | 24 | 41.00 |
| mmu05161 | Hepatitis B | 8.6e-06 | 98 | 163.00 |
| mmu05100 | Bacterial invasion of epithelial cells | 1.4e-05 | 46 | 76.00 |

| | | | | |
|---|---|---|---|---|
| mmu05217 | Basal cell carcinoma | 2.1e-05 | 37 | 63.00 |
| mmu04213 | Longevity regulating pathway - multiple species | 3.6e-05 | 37 | 62.00 |
| mmu00330 | Arginine and proline metabolism | 5.0e-05 | 29 | 54.00 |
| mmu01524 | Platinum drug resistance | 7.2e-05 | 44 | 0.00 |
| mmu00670 | One carbon pool by folate | 9.5e-05 | 14 | 19.00 |

## G.3 Pathways enriched in human versus mouse ectoderm derived tissue groups

*Comparison 3: Human versus mouse ectoderm derived tissue groups.* For this comparison, like previous study we obtained 7,037 coinciding genes among all datasets. Since the genes belong to both human and mouse data. We obtained 58 enriched pathways post Bonferroni correction (Dunnett, 1955) ($P \leq 0.05$) for human using SIGORA analysis and human KEGG repository (Kanehisa and Goto, 2000). We obtained 26 enriched pathways post Bonferroni correction (Dunnett, 1955) ($P \leq 0.05$) for mouse using mouse KEGG repository (Kanehisa and Goto, 2000). We report 23 intersecting enriched pathways from human and mouse. Table S7, shows all 23 enriched pathways with Kegg pathway id of human and mouse, description, the Bonferroni adjusted p-value, number of successes and the pathway size of both human and mouse.

Table S7: Biological pathways enriched with rewired second-order gene-gene differential patterns between human and mouse ectoderm.

| Human Pathway ID | Mouse Pathway ID | Description | Bonferroni (hsa) | Successes (hsa) | Pathways Size (hsa) | Bonferroni (mmu) | Successes (mmu) | Pathways Size (mmu) |
|---|---|---|---|---|---|---|---|---|
| hsa04010 | mmu04010 | MAPK signaling pathway | 0.0e+00 | 172 | 294.00 | 0.0e+00 | 172 | 294.00 |
| hsa04110 | mmu04110 | Cell cycle | 0.0e+00 | 83 | 124.00 | 4.2e-284 | 83 | 123.00 |
| hsa04360 | mmu04360 | Axon guidance | 0.0e+00 | 129 | 181.00 | 0.0e+00 | 129 | 180.00 |
| hsa04144 | mmu04144 | Endocytosis | 2.2e-281 | 126 | 252.00 | 8.0e-94 | 127 | 273.00 |
| hsa04310 | mmu04310 | Wnt signaling pathway | 1.9e-223 | 94 | 160.00 | 1.4e-127 | 93 | 162.00 |
| hsa04142 | mmu04142 | Lysosome | 5.2e-191 | 70 | 128.00 | 2.3e-111 | 70 | 131.00 |
| hsa05205 | mmu05205 | Proteoglycans in cancer | 6.0e-180 | 123 | 205.00 | 1.3e-132 | 125 | 205.00 |
| hsa04530 | mmu04530 | Tight junction | 4.4e-176 | 97 | 169.00 | 2.4e-140 | 97 | 167.00 |
| hsa04014 | mmu04014 | Ras signaling pathway | 1.2e-158 | 128 | 232.00 | 1.9e-115 | 127 | 232.00 |
| hsa04910 | mmu04910 | Insulin signaling pathway | 1.2e-146 | 86 | 137.00 | 1.8e-111 | 87 | 139.00 |
| hsa04015 | mmu04015 | Rap1 signaling pathway | 9.3e-146 | 128 | 210.00 | 1.1e-98 | 128 | 214.00 |
| hsa04141 | mmu04141 | Protein processing in endoplasmic reticulum | 2.4e-124 | 86 | 171.00 | 2.3e-67 | 86 | 172.00 |
| hsa00564 | mmu00564 | Glycerophospholipid metabolism | 1.5e-103 | 54 | 98.00 | 1.2e-69 | 54 | 98.00 |
| hsa04068 | mmu04068 | FoxO signaling pathway | 2.3e-102 | 82 | 131.00 | 6.2e-74 | 81 | 131.00 |
| hsa05202 | mmu05202 | Transcriptional misregulation in cancer | 7.9e-95 | 90 | 192.00 | 8.0e-60 | 90 | 223.00 |
| hsa04390 | mmu04390 | Hippo signaling pathway | 1.4e-89 | 93 | 157.00 | 4.3e-61 | 93 | 157.00 |
| hsa04810 | mmu04810 | Regulation of actin cytoskeleton | 1.3e-87 | 124 | 218.00 | 3.8e-55 | 124 | 220.00 |
| hsa04210 | mmu04210 | Apoptosis | 5.3e-84 | 82 | 136.00 | 1.6e-61 | 82 | 136.00 |
| hsa04350 | mmu04350 | TGF-beta signaling pathway | 3.7e-80 | 52 | 94.00 | 4.5e-40 | 51 | 95.00 |
| hsa03030 | mmu03030 | DNA replication | 1.1e-74 | 28 | 36.00 | 1.3e-66 | 28 | 35.00 |
| hsa04710 | mmu04710 | Circadian rhythm | 5.3e-71 | 25 | 31.00 | 1.1e-57 | 24 | 30.00 |
| hsa05412 | mmu05412 | Arrhythmogenic right ventricular cardiomyopathy (ARVC) | 7.6e-69 | 52 | 77.00 | 1.3e-55 | 52 | 77.00 |
| hsa04070 | mmu04070 | Phosphatidylinositol signaling system | 2.8e-66 | 65 | 97.00 | 1.4e-50 | 65 | 96.00 |

## G.4 Pathways enriched in human versus mouse primitive streak derived tissue groups

*Comparison 4: Human versus mouse primitive streak derived tissue groups.* We obtained 3,357 coinciding genes involved in second-order differential patterns among all datasets. We obtained 14 enriched pathways post Bonferroni correction (Dunnett, 1955) ($P \leq 0.05$) for human using SIGORA analysis and human KEGG repository (Kanehisa and Goto, 2000). We obtained 7 enriched pathways post Bonferroni correction (Dunnett, 1955) ($P \leq 0.05$) for mouse using mouse KEGG repository (Kanehisa and Goto, 2000). We report six intersecting enriched pathways from human and mouse. Table S8, shows all six enriched pathways with Kegg pathway id of human and mouse, description, the Bonferroni adjusted p-value, number of successes and the pathway size of both human and mouse.

Table S8: Biological pathways enriched with rewired second-order gene-gene differential patterns between human and mouse primitive streak.

| **Human Pathway ID** | **Mouse Pathway ID** | **Description** | **Bonferroni (hsa)** | **Successes (hsa)** | **Pathways Size (hsa)** | **Bonferroni (mmu)** | **Successes (mmu)** | **Pathways Size (mmu)** |
|---|---|---|---|---|---|---|---|---|
| hsa04144 | mmu04144 | Endocytosis | 1.2e-231 | 74 | 252.00 | 8.3e-129 | 74 | 273.00 |
| hsa04110 | mmu04110 | Cell cycle | 1.3e-194 | 52 | 124.00 | 8.8e-170 | 52 | 123.00 |
| hsa04360 | mmu04360 | Axon guidance | 3.0e-135 | 57 | 181.00 | 4.6e-100 | 58 | 180.00 |
| hsa04146 | mmu04146 | Peroxisome | 9.8e-133 | 36 | 83.00 | 1.5e-109 | 36 | 86.00 |
| hsa00280 | mmu00280 | Valine, leucine and isoleucine degradation | 4.3e-89 | 30 | 48.00 | 1.2e-66 | 30 | 57.00 |
| hsa04530 | mmu04530 | Tight junction | 3.2e-79 | 53 | 169.00 | 1.1e-70 | 53 | 167.00 |

# H Detecting rewired miRNA–gene patterns between developing mouse cerebellum and liver

## H.1 Preparation of FANTOM5 developing mouse cerebellum and liver data

We prepared FANTOM5 developing mouse cerebellum and liver data as follows. *Sample selection:* Cerebellum had 37 samples over 13 developmental time points with 3 replicates for the first 12 time points (E11 to N09) and one replicate for N30. Liver had 15 samples over 15 development time points. *Usage of microRNA (miRNA):* FANTOM Consortium (2017) measured TPMs of 641 pri-miRNAs, with names of their host genes, across all 1029 matching samples from the mouse dataset. They found that pri-miRNAs are co-expressed with mature miRNA and suggested pri-miRNAs as a proxy to mature miRNAs. *Pre-processing:* We started with TPMs of two datasets containing 641 pri-miRNAs and 22,637 p1 TSSs across 37 cerebellum samples and that across 15 liver samples. Each dataset was found to be fairly normally distributed. Thus, we did not log scale the data. N30 in cerebellum was often recognized as an outlier and removed. Mostly unchanged TSSs and pri-miRNAs with MAD (median absolute deviation) at the bottom 5% were removed from both datasets. After preprocessing, we obtain 12,937 TSSs and 502 pri-miRNAs for 36 cerebellar samples and 15 liver samples. We than constructed co-expression networks for both tissue types evaluating $502 \times 12{,}937$ patterns using second-order network rewiring pipeline. We obtained 20,577 significant patterns in cerebellum and 197,347 in liver. A union of 216,709 unique patterns were supplied to the Sharma-Song test that returned 42,352 significant (Benjamini-Hochberg adjusted $P < 0.05$ and $\varepsilon > 0.456$) 2nd-order differential patterns. Figure S3 shows five second-order differential patterns.

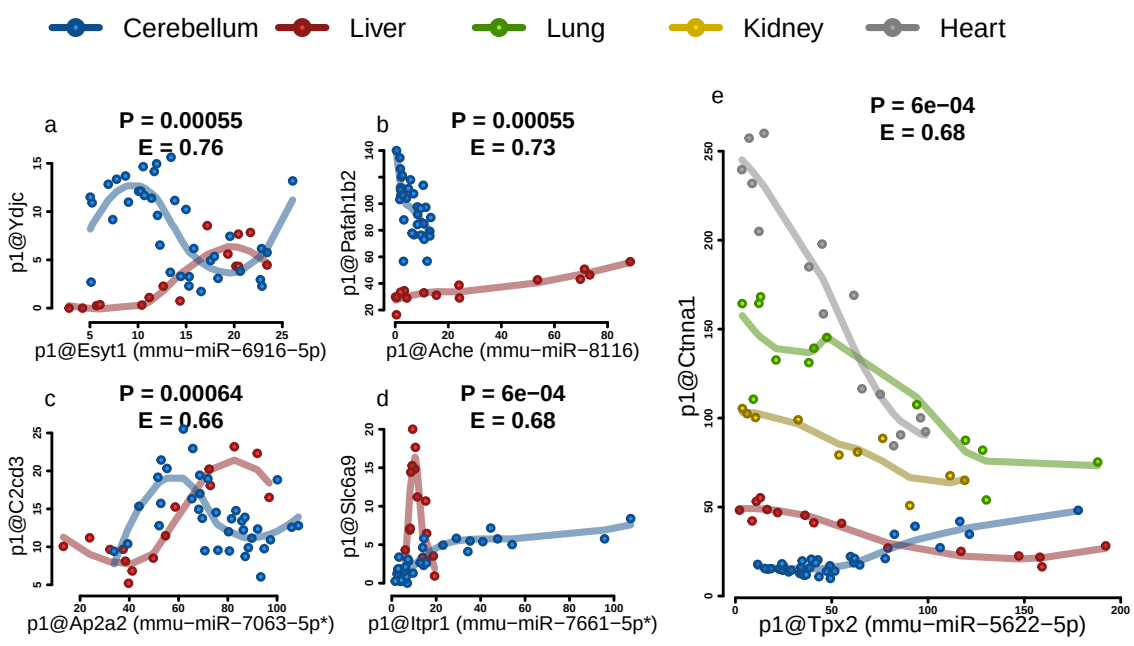


**Fig. S3. Detected 2nd-order differential miRNA–gene patterns across developing mouse cerebellum, liver, lung, kidney, and heart by the Sharma-Song test.** Each point represents one tissue sample. The horizontal axis is an miRNA with both promoter and miRNA names, and the vertical axis the TSS of a gene. A curve is fitted to sample points of each tissue type by loess to summarize the dynamics. (a)–(d), four miRNA–gene pairs that are 2nd-order differential between developing cerebellum and liver. (e), a pattern that is 2nd-order differential between developing cerebellum and all other tissue types.

## H.2 Biological pathways enriched with rewired second-order miRNA-gene differential patterns between developing cerebellum and liver in mice

Second-order differential patterns (42,352) (Benjamini-Hochberg adjusted $P < 0.05$ and $\varepsilon > 0.4565$) were selected with 5,888 unique TSSs. A SIGORA (Foroushani et al., 2013) analysis on the TSSs returned 12 enriched pathways post Bonferroni correction (Dunnett, 1955). The top pathways spliceosome (mmu03040), RNA-transport (mmu03013), and cell-cycle (mmu04110), all critical in development. Spliceosome is a large nuclear machinery responsible for splicing. Alternate splicing is critical in cellular differentiation and organism development, collaborating with other components to generate abundant protein diversity (Wang et al., 2015). This diversity can lead to mechanistic rewiring. For example, alternative splicing events can rewire transcriptional control (Will and Helms, 2017). The RNA-transport pathway is functionally coupled with transcription, splicing, 3'-end formation and translation (Kanehisa and Goto, 2000), all of which are prone to rewiring. Cell cycles are closely coupled with cellular differentiation where development signals often determine cell cycle mode specific to cell type (Jakoby and Schnittger, 2004), subject to tissue specific rewiring. For example, in some brain regions, the orientation of granule cell precursor division can determine the production of more granule cell precursors or granule cells (Miyashita et al., 2017).

Liver and cerebellum specific pathways are also enriched with 2nd-order rewiring. The glycerophospholipid metabolism pathway is involved in hen's liver development (Li et al., 2015). Its dysfunction in rat was associated with liver fibrosis development (Wang et al., 2016), suggesting its importance in maintaining hepatic homeostasis.

Such biological evidence supports the effectiveness of Sharma-Song test to implicate rewired pathways critical for tissue-specific development.

Table S9. **Biological pathways enriched with rewired second-order miRNA-gene differential patterns between developing mouse cerebellum and liver.**

| Pathway ID | KEGG pathway name | $P$-value | Successes | Pathway size |
|---|---|---|---|---|
| mmu03013 | RNA transport | 0.0e+00 | 79 | 182.00 |
| mmu03040 | Spliceosome | 0.0e+00 | 67 | 136.00 |
| mmu04141 | Protein processing in endoplasmic reticulum | 0.0e+00 | 75 | 172.00 |
| mmu04110 | Cell cycle | 2.9e-206 | 67 | 123.00 |
| mmu03030 | DNA replication | 4.0e-142 | 31 | 35.00 |
| mmu04146 | Peroxisome | 4.1e-111 | 43 | 86.00 |
| mmu04218 | Cellular senescence | 6.8e-108 | 76 | 185.00 |
| mmu04144 | Endocytosis | 5.3e-98 | 100 | 273.00 |
| mmu00280 | Valine, leucine and isoleucine degradation | 5.4e-91 | 37 | 57.00 |
| mmu04142 | Lysosome | 9.2e-87 | 55 | 131.00 |
| mmu00564 | Glycerophospholipid metabolism | 1.6e-45 | 36 | 98.00 |
| mmu04360 | Axon guidance | 8.4e-34 | 69 | 180.00 |

**Pathway ID** is the KEGG ID of a pathway. **KEGG pathway name** is the name of a pathway in KEGG. $P$**-value** is the adjusted enrichment $P$-values obtained from SIGORA. **Successes** is the number of genes involved in 2nd-order differential patterns found in the selected pathway. **Pathway size** is the total number of genes belonging to the selected pathway.

## H.3 Second-order differential network of spliceosome pathway between developing cerebellum and liver in mice

We expand on the top pathway–spliceosome (mmu03040) by building a 2nd-order differential network between developing cerebellum and liver using the Sharma-Song test. A sub-network is shown in Figure S4 consisting of 12 second-order gene-gene patterns (edges) out of 200 patterns. Top five hub TSSs ranked by their degrees are highlighted, along with other nodes. A total of 136 TSSs involved in the spliceosome KEGG pathway (Kanehisa and Goto, 2000) were extracted using the R package 'KEGGREST' (Tenenbaum, 2016). Only 112 TSSs out of 132 had p1 profiles available in mouse FANTOM5. We selected 104 high dynamic TSSs using MAD(median absolute deviation). We followed the second-order network rewiring pipeline to build cerebellum and liver specific co-expression networks using $104\times104$ co-expression patterns. We found 78 significant patterns in cerebellum and 612 patterns in liver. A union of 677 patterns were given to the Sharma-Song test which returned 42 significant (Benjamini-Hochberg adjusted $P$<0.05 and $\varepsilon$>0.456) 2nd-order differential patterns. Hub genes were identified by a high degree of connections, out of which *Sf3a3*, *Sf3a1*, *Snrpa1*, *Sf3b3*, *Dhx15*, *Lsm2* and *U2af2*, stood out with each having more than 20 degrees. The seven hub genes accounted for a total 200 (out of 677) edges, including 12 (out of 42) 2nd-order differential edges, presented in Figure S4.

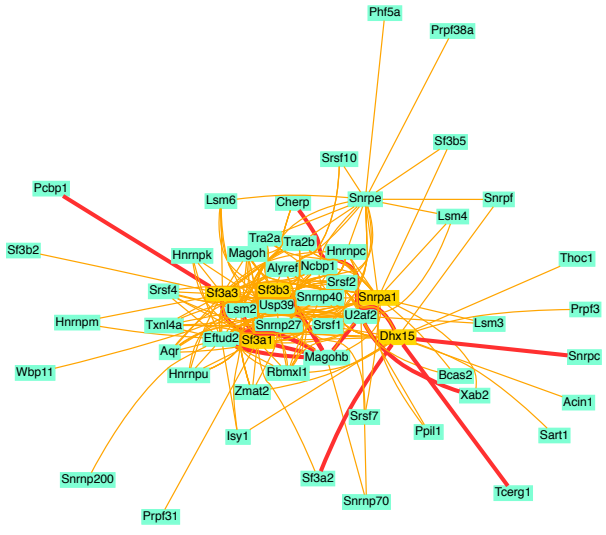


**Fig. S4. A spliceosome second-order differential co-expression sub-network featuring 200 patterns (edges) across top hub genes in developing mouse cerebellum and liver tissues.** The orange edges represent significant co-expression patterns among transcripts (aquamarine). The top five hub genes, ranked by their degree, are represented in gold. Edges representing 2nd-order changes between cerebellum and liver are highlighted in red.

## I Benchmarking the Sharma-Song test for differential patterns across three conditions

We conducted simulation study with similar experimental design as given in the Results section 3.4. The difference is that we use $K = 3$ experimental conditions here instead of $K = 2$ in section 3.4. We did not include the DGCA method as its core statistic was not designed for over two conditions, which could be extended to three conditions. However, we saw from the previous study that differential correlation and DGCA had almost the same performance. Again, we observed the substantially better performance of Sharma-Song test over the heterogeneity test and differential correlation. The result is shown in Figure S5.

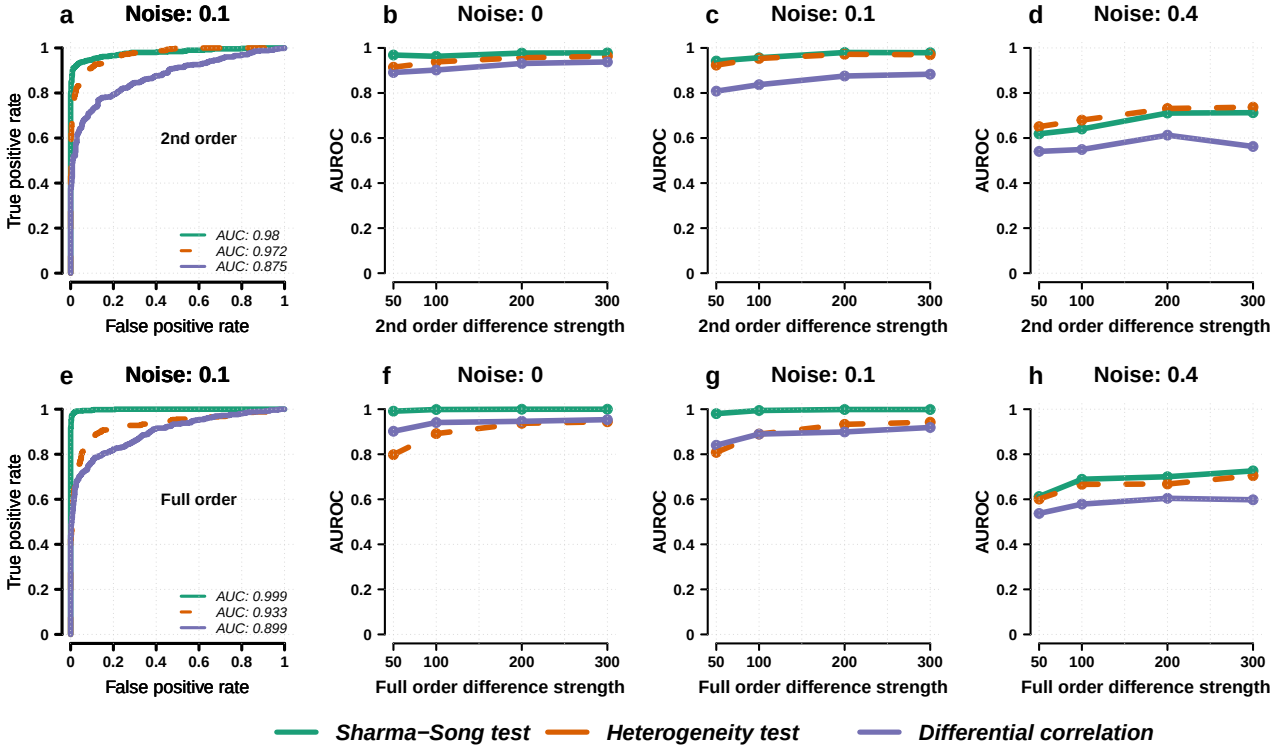


**Fig. S5. Benchmarking the Sharma-Song test and three other methods.** (a), ROC curve at noise level 0.1 for the 2nd-order study. (b, c, d), AUROC (Y-axis) at noise levels 0, 0.1 and 0.4 with increasing strength of differentiality (X-axis) of 2nd-order differential tables. (e), ROC curve at noise level 0.1 for the full-order differential study. (f, g, h), AUROC (Y-axis) at noise levels 0, 0.1 and 0.4 with increasing strength of differentiality (X-axis) of full-order differential tables.

## J The statistical power of the Sharma-Song test

The statistical power of the Sharma-Song test as a function of sample size given false positive rate, effect size, and table size is shown in Figure S6. To estimate the effect size cutoff of 0.23, we used the thresholding strategy mentioned earlier for fixed 3×3, 4×4 and 5×5 table sizes, by simulating 100,000 differential patterns for each table size across two conditions with 50 samples in each condition. Finally, we took the median of their effect sizes at 60% thresholds. The following procedure was used to compute the statistical power in relation to sample size:

1. For each table size $r \times s$, we simulated the alternative population at sample sizes between 3 to 100, with the requirement that a sample size $n$ is no smaller than $r$;
2. For each valid sample size $n$, the alternative population was generated by simulating 100,000 discrete differential co-expression patterns in two experimental conditions;
3. Differential co-expression patterns were simulated using `simulate_tables` (Sharma et al., 2017) in the 'FunChisq' R package where we generated two contingency tables each with $r$ rows, $s$ columns and $n$ samples;
4. Each table was randomly selected to carry either a functional, a dependent but non functional or an independent relationship, however, for $n < r \cdot s$, each table could only carry a functional or an independent relationship, as per the minimum requirements for non-functional dependent relationships in `simulate_tables`. A table pair $\mathbf{C}_1, \mathbf{C}_2$ was considered differential if their weighted cell-wise difference $\Delta p$ was found to be larger than 2.2e-16, where $\Delta p$ was calculated as:

$$\Delta p = \sum_{i=1}^{r} \sum_{j=1}^{s} \left| \frac{\mathbf{C}_1[i,j] - \bar{\mathbf{C}}_1[i,j]}{n} - \frac{\mathbf{C}_2[i,j] - \bar{\mathbf{C}}_2[i,j]}{n} \right| \tag{S15}$$

   where $\bar{\mathbf{C}}_1$ and $\bar{\mathbf{C}}_2$ are the expected count matrices defined in the main text;
5. Once we obtained the alternative population for a given table and sample size, we applied Sharma-Song test on all 100,000 differential patterns. To calculate the statistical power, the ground truth tables were determined to be those with an effect size $\varepsilon$>0.23, irrespective of their Sharma-Song $P$-value. The true-positive cases were determined to be those among the ground-truth tables with a Sharma-Song $P$<0.05.

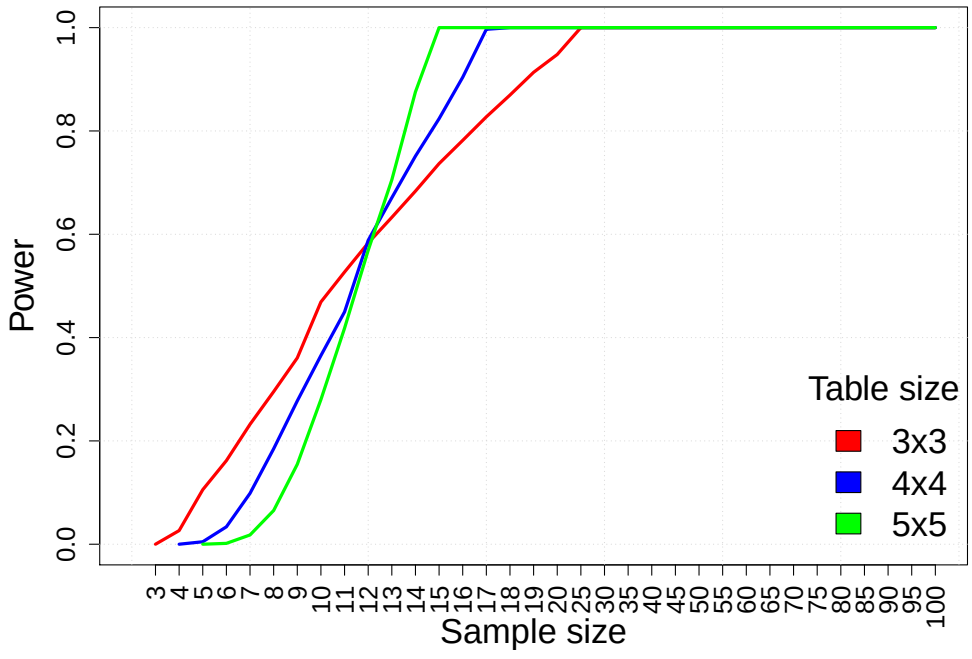


**Fig. S6.** **The statistical power of Sharma-Song test as a function of sample size given false positive rate 0.05, effect size $\varepsilon_{60}$, and table size. The horizontal axis represents the sample size. The vertical axis represents the statistical power (true positive rate). The three curves stand for the power given table dimensions of 3×3 (red), 4×4 (blue) and 5×5 (green).**

## References

Dunnett, C. W. (1955). A multiple comparison procedure for comparing several treatments with a control. *J Am Stat Assoc*, 50(272):1096–1121.

FANTOM Consortium (2017). An integrated expression atlas of miRNAs and their promoters in human and mouse. *Nat Biotechnol*, 35(9):872–878.

Foroushani, A. B., Brinkman, F. S., and Lynn, D. J. (2013). Pathway-GPS and SIGORA: identifying relevant pathways based on the over-representation of their gene-pair signatures. *PeerJ*, 1:e229.

Jakoby, M. and Schnittger, A. (2004). Cell cycle and differentiation. *Current Opinion in Plant Biology*, 7(6):661–669.

Kanehisa, M. and Goto, S. (2000). KEGG: Kyoto encyclopedia of genes and genomes. *Nucleic Acids Research*, 28(1):27–30.

Lancaster, H. O. (1949). The derivation and partition of $\chi^2$ in certain discrete distributions. *Biometrika*, 36(1/2):117–129.

Li, H., Wang, T., Xu, C., Wang, D., Ren, J., Li, Y., Tian, Y., Wang, Y., Jiao, Y., Kang, X., and Liu, X. (2015). Transcriptome profile of liver at different physiological stages reveals potential mode for lipid metabolism in laying hens. *BMC Genomics*, 16(1):763.

McLachlan, G. J. (1999). Mahalanobis distance. *Resonance*, 4(06):20–26.

Miyashita, S., Adachi, T., Yamashita, M., Sota, T., and Hoshino, M. (2017). Dynamics of the cell division orientation of granule cell precursors during cerebellar development. *Mech Dev*, 147:1–7.

Sharma, R., Kumar, S., Zhong, H., and Song, M. (2017). Simulating noisy, nonparametric, and multivariate discrete patterns. *R J*, 9(2):366–377.

Song, M. and Zhong, H. (2020). Efficient weighted univariate clustering maps outstanding dysregulated genomic zones in human cancers. *Bioinformatics*, 36(20):5027–5036.

Tenenbaum, D. (2016). KEGGREST: Client-side REST access to KEGG. R package version 1.30.0.

Wang, G., Li, Z., Li, H., Li, L., Li, J., and Yu, C. (2016). Metabolic profile changes of CCl4-liver fibrosis and inhibitory effects of Jiaqi Ganxian granule. *Molecules*, 21(6):698.

Wang, H. and Song, M. (2011). Ckmeans.1d.dp: Optimal $k$-means clustering in one dimension by dynamic programming. *R J*, 3(2):29–33.

Wang, Y., Liu, J., Huang, B. O., Xu, Y.-M., Li, J., Huang, L.-F., Lin, J., Zhang, J., Min, Q.-H., Yang, W.-M., and Wang, X.-Z. (2015). Mechanism of alternative splicing and its regulation. *Biomed Rep*, 3(2):152–158.

Will, T. and Helms, V. (2017). Rewiring of the inferred protein interactome during blood development studied with the tool PPICompare. *BMC Syst Biol*, 11(1):44.